

SURFACE IMAGE VELOCIMETRY USING INFRARED IMAGING

by

Ethan W. Jackson

A THESIS

Presented to the Faculty of

The Graduate College at the University of Nebraska

In Partial Fulfillment of the Requirements

For the Degree of Master of Science

Major: Electrical Engineering

Under the Supervision of Professor David Admiraal and Professor Dennis Alexander

Lincoln, Nebraska

December 2009

SURFACE IMAGE VELOCIMETRY USING INFRARED IMAGING

Ethan W. Jackson, M.S.

University of Nebraska, 2009

Advisor: David Admiraal and Dennis Alexander

The purpose of this project was to develop a method of measuring surface velocity and discharge in water bodies using an infrared (IR) camera. Two laboratory experiments and field exercises were performed in channels of varying sizes and flow rates. Flow rates calculated with the IR camera were compared to the known flow rates of the channels for accuracy assessment. Development of this method will allow for a less intrusive measurement technique that can be easily mobilized.

Data collected from the IR camera were converted from the raw data to surface velocity distributions of the water body using specially developed software. The software allowed oblique images to be rectified, producing plan view images of the water surface. The corrected images could then be compared to each other by the software to calculate the water surface velocity distributions. It was found that if the contrast of the temperature structures on the surface of the water were too low compared to bank reflections, velocity calculations were biased to zero. Reflections played a much more significant role when the water was cold relative to the banks than when it was warm relative to the banks. When reflections were not a problem, averaging data showed that velocity averages from 50 pairs of images provided a reasonable approximation of the actual average discharge in a channel. The accuracy of the average discharge calculation improved if 100 to 115 pairs of images were averaged, but beyond this number, additional image pairs did not substantially improve the result. Finally, it was found that thermal structures must move a significant distance between images belonging to an image pair. If the thermal structures do not move far between images, the result is much more likely to be biased to zero by image reflections.

Acknowledgement of Project Support

This work is part of a project sponsored by the Nebraska Public Power District (NPPD) through the Nebraska Center for Energy Sciences Research (NCESR). I would like to thank NPPD and NCESR not only for funding the project, but also for being extremely helpful in establishing contacts, providing research ideas and guidance, and allowing us to work on property owned by NPPD. I would also like to thank the Water Center of the University of Nebraska – Lincoln for allowing us to use the thermal camera purchased by the Water Center. We would not have been able to complete this project without the support of these three organizations.

Acknowledgements

I would like to thank Dr. Dennis R. Alexander for talking me into going for my master's degree, and also for guiding me through graduate school.

I would also like to thank David M. Admiraal for his immense amounts of help with the research and writing.

I especially want to thank my wife Sara for putting up with me.

Table of Contents

Acknowledgement of Project Support	iii
Acknowledgements	iv
Table of Contents	v
List of Figures.....	vii
List of Tables	xi
List of Appendices.....	xiii
Notation.....	xiv
Chapter 1. Introduction.....	1
1.1 Project Overview	1
1.2 Project Objectives.....	1
1.2.1 Objectives for this project.....	1
1.2.2 Future objectives and possible uses for techniques used.....	2
1.3 Thesis Chapter Overview.....	2
Chapter 2. Literature Review	3
2.1 Introduction.....	3
2.2 Water Surface Temperature Tracking.....	3
2.3 Techniques Used.....	7
2.4 Particle Image Velocimetry (PIV) Methods	8
Chapter 3. Instrumentation	11
3.1 Introduction.....	11
3.2 Infrared Camera System	12
3.3 Total Station.....	16
3.4 Acoustic Doppler Velocimeter	18
3.5 Point Gages	20
3.6 V-notch Weir	21
3.7 Acoustic Doppler Current Profiler.....	22
Chapter 4. Data Collection and Experimental Procedure	24
4.1 Data Collection Overview	24
4.2 70-cm Flume Test.....	24
4.3 240-cm Flume Test.....	27
4.4 Transposition of Position Reference Points onto Large Water Surfaces.....	33
4.5 The Irrigation Canal at Canaday Station.....	36
4.6 Lake Ogallala	39

4.7 Sutherland Reservoir Cooling Pond Inflow Canal above Drop Structure	43
4.8 Sutherland Reservoir Cooling Pond Outlet	44
4.9 Sutherland Reservoir Outlet Canal	45
4.9.1 Top view from the bridge above the canal.....	47
4.9.2 Upstream view of the canal.....	49
4.9.3 Side view of the canal	50
Chapter 5. Data Analysis Program and Process	52
5.1 Introduction.....	52
5.2 Image Processing Procedure.....	52
5.3 Processing Procedure for Images Collected From the Side of the Canal	53
5.4 Side View Processing Results, August 2008.....	61
5.5 Flow Rate Comparisons, August 2008	67
5.6 Side View Processing Results and Comparison, July 2009.....	70
Chapter 6. Conclusions.....	76
6.1 Overview.....	76
6.2 General conclusions.....	76
6.3 Implications for future research.....	78
References.....	79

List of Figures

Figure 2.1 Absorption coefficient of water for selected ranges of infrared light (after McAlister, 1964).	4
Figure 2.2 Spectral emissivity of water in the infrared region for selected angles of view. Probability scale (after Bramson, 1968)	5
Figure 3.1 ThermaCAM S65HSV (www.flirthermography.com, 2009)	14
Figure 3.2 An example of ThermaCAM software GUI.	15
Figure 3.3 Sokkia total station	17
Figure 3.4 ADV system with the probe in center, the conditioning module on bottom and the signal processor on top.	19
Figure 3.5 Close-up of the ADV probe. (www.sontek.com, 2009)	19
Figure 3.6 (a) Example of a point gage used. (b) Close up of point gage.	20
Figure 3.7 The V-Notch weir used to measure discharges in the lab.	22
Figure 3.8 Workhorse Rio Grande 1200 kHz ADCP	23
Figure 4.1 Small flume experimental setup	25
Figure 4.2 Thermal images showing seeded water moving through the measurement region for Test A. 3.1.	27
Figure 4.3 240-cm wide flume test setup.	29
Figure 4.4 Thermal image of grid used to correct image distortion	30
Figure 4.5 Thermal image showing water surface in the 240-cm flume without seeding	31
Figure 4.6 Thermal image showing water flowing in the 240-cm flume with the laser pointed at a fixed surface position	32

Figure 4.7 Thermal image showing water flowing in the 240-cm flume with the laser sweeping 30 cm across the surface at a frequency of 0.5 Hz.....	32
Figure 4.8 Thermal image showing water flowing in the 240-cm flume with the laser sweeping 25 cm across the surface at a frequency of 1.0 Hz.....	33
Figure 4.9 Rotational transposition of image calibration control points	35
Figure 4.10 Aerial photograph of Canaday Station location with the hot water discharge near the bridge on the left, and a second bridge on the right. (Canaday Station outlet canal, maps.google.com, Aug, 2009).....	36
Figure 4.11 Discharge channel leading to the canal.	37
Figure 4.12 Downstream view of the irrigation canal.	37
Figure 4.13 Upstream view of irrigation canal.	38
Figure 4.14 Aerial image of the inlet of Lake Ogallala showing the location of the position reference points and camera. (Lake Ogallala inlet, maps.google.com, Aug, 2008)	40
Figure 4.15 Thermal image of the north shore of the Lake Ogallala Inlet	41
Figure 4.16 Thermal image of the center of the Lake Ogallala inlet.....	41
Figure 4.17 Thermal image of the south shore of the Lake Ogallala inlet	42
Figure 4.18 Map locating the three sites considered at Sutherland Reservoir. (Sutherland Reservoir, maps.google.com, Aug, 2009).....	43
Figure 4.19 Inflow canal above the drop structure.	44
Figure 4.20 Sutherland reservoir cooling pond outlet.	45
Figure 4.21 Aerial photograph of the outlet from Sutherland Reservoir. (Sutherland Reservoir outlet canal, maps.google.com, Aug, 2008)	46

Figure 4.22 Sample image showing temperature differences in water below the bridge.	48
Figure 4.23 Thermal image showing measurement calibration marker	49
Figure 4.24 Thermal image of the NPPD Power Canal looking upstream from the bridge with the three position reference points used in 2008 marked.....	50
Figure 4.25 Thermal image taken from the side of the canal with nine position reference points marked.....	51
Figure 5.1 Sample of batch alignment dialog in FFCMD	54
Figure 5.2 Oblique image correction coefficients table.....	55
Figure 5.3 Test image showing position reference point locations	56
Figure 5.4 Dialog to specify image properties of rectified oblique images.....	57
Figure 5.5 Oblique image of canal that has been rectified	58
Figure 5.6 Demonstration of batch processing table	59
Figure 5.7 Rectified images, including unfiltered (left) and filtered (right) images.....	60
Figure 5.8 Demonstration of Image Velocimetry batch table.....	61
Figure 5.9 No filter, 33ms separation	62
Figure 5.10 Filtered, 33ms separation.....	62
Figure 5.11 No filter, 66ms separation	63
Figure 5.12 Filtered, 66ms separation.....	63
Figure 5.13 No filter, 99ms separation	63
Figure 5.14 Filtered, 99ms separation.....	63
Figure 5.15 No filter, 132ms separation	64
Figure 5.16 Filtered, 132ms separation.....	64

Figure 5.17 Depth profile of the NPPD power canal downstream of Sutherland Reservoir (NPPD, 2008).....	65
Figure 5.18 Average discharge for 50 sets of images for three transect rows. a through c show unfiltered data and d through f show filtered data.....	66
Figure 5.19 Number of image pairs required to stabilize the results for filtered image pairs in run 230.	70
Figure 5.20 Discharge average of 50 sets of images for the first transect row.....	71
Figure 5.21 (a) Image with good vector plots with few variations in magnitude and direction. (b) Image with poor vector plots with large variation in magnitude and direction.	73
Figure 5.22 (a) Image showing few reflections with the banks cooler than the water. (b) Image showing reflections with the banks warmer than the water.....	74

List of Tables

Table 3.1 ThermaCam S65HSV Technical Specifications (FLIR Systems, 2006)	13
Table 3.2 ADV Technical Specifications (SonTek Manual 1997).....	18
Table 5.1: Percentage difference of calculated flow to actual flow of 1415 cfs.....	69
Table 5.2: Percentage difference of calculated flow to actual flow of 1160 cfs.....	72
Table A.1: Flow rate average of the runs, measured using the V-notch Weir.....	A.2
Table A.1: (Continued).....	A.3
Table A.1: (Continued).....	A.4
Table A.1: (Continued).....	A.5
Table B.2: ADV Data	B.2
Table B.3: Large flume flow and depth data	B.3
Table C.1: Ogallala Inlet Total Station Calibration Measurements August 2008	C.2
Table C.2: Ogallala Inlet GPS Coordinates August 2008.....	C.2
Table C.3: Sutherland Reservoir Outlet Total Station Points for Upstream Images August 2008.....	C.2
Table C.4: Sutherland Reservoir Outlet Total Station Points for Side Images August 2008	C.3
Table C.5: Average discharge of 50 sets for every test run August 2008	C.3
Table C.5: (Continued).....	C.4
Table C.6: Sutherland Reservoir Outlet Total Station Points for Side Images July 2009	C.5
Table C.7: Sutherland Reservoir Outlet GPS Coordinates July 2009	C.5
Table C.8: Average discharge of 50 sets for every test run July 2009	C.6

Table C.8: (Continued)C.6

Table C.8: (Continued)C.7

Table C.9: Three supplemental position reference points with prism held over the water
in view of the infrared camera July 2009.....C.7

List of Appendices

- A. Small Flume Flow Rate Data
- B. Large Flume Flow Rate Data
- C. Position reference point Data

Notation

Symbol No.	Symbol/Variable	Description
1	IR	Infrared
2	PIV	Particle Image Velocimetry
3	Hz	Frequency
4	MQD	Minimum quadratic difference
5	D(m,n)	Displacement of the tracked pattern
6	M	Pixel size in x direction
7	N	Pixel size in y direction
8	M	Initial M location
9	N	Initial N location
10	g(i)	Movement along x
11	g(j)	Movement along y
12	NPPD	Nebraska Public Power District
13	ADCP	Acoustic doppler current profiler
14	.fpf	Flir public format
15	ADV	Acoustic doppler velocimeter
16	Q	Water flow rate / discharge
17	C _D	Discharge coefficient
18	G	Gravitational acceleration
19	H	Height of water over weir crest
20	θ	Angle of the V-notch weir
21	FFCMD	Flow field captor MD
22	dT	Time separation between images

Chapter 1. Introduction

1.1 Project Overview

Over the past decade, infrared (IR) cameras have become more widely available, more accurate, more sensitive and less costly. The sensitivity of commercially available IR cameras has become such that it is possible to easily track thermal structures on the surface of a water body. In this thesis, the motion of natural thermal structures and thermal structures injected from warm water sources into water bodies is tracked to measure surface velocities. The result is a velocity profile of the water surface, which in many situations can be used to calculate channel discharges.

1.2 Project Objectives

The goal of this research was to develop a method to track surface velocities of a water body using thermal imaging. An IR camera was used to gather thermal images of the water surface. Algorithms were then developed that allow for the conversion of thermal images into velocity distributions for the surface of the water body.

1.2.1 Objectives for this project

The following objectives were identified for the work described in this thesis:

1. Optimize methods for viewing and tracking the surface structures on a water body using an IR camera.
2. Develop algorithms that will accurately convert thermal images into velocity vectors over the surface of the water body.

3. Extend the use of the IR camera for measuring velocities in non laboratory settings, correcting for oblique camera angles, and using natural markers for distance recognition.

1.2.2 Future objectives and possible uses for techniques used

The following objectives were developed for future implementation of the PIV technique presented in this thesis:

1. Refine the accuracy of the methods used to collect and process the thermal imagery.
2. Develop methods for getting position reference points without being near the water.

1.3 Thesis Chapter Overview

The chapters for this thesis have been developed to cover the important aspects of the project and are sequenced to build towards the concluding chapters that contain the results found from the data gathered in the research. These chapters include the following:

- Chapter 2. Literature Review. This chapter describes previous methods used for tracking water surface velocities using various gradient measurement methods.
- Chapter 3. Instrumentation. In this chapter the types of instrumentation used, the accuracies of the instruments, and how the instruments are used are discussed.
- Chapter 4. Data collection and experimental procedure. The methods used to collect the data presented in this thesis are discussed in this chapter.
- Chapter 5. Data analysis processes. Here the methods used for extracting information from the raw data and turning it into usable information are discussed.
- Chapter 6. Conclusions and implications for future research.

Chapter 2. Literature Review

2.1 Introduction

There has been much research and study done measuring surface velocities of water and calculating the discharge of the water body from those measurements. Much of this research is based on Particle Image Velocimetry (PIV) that relies on particles being suspended in or floating on the water body that is being tracked. Using a thermal camera will allow for tracking of surface structures on the water based on variations of the surface temperature instead of having to rely on seeding the flow.

2.2 Water Surface Temperature Tracking

Measuring the motion of a water surface using thermal imaging is a relatively new procedure. The tracking of the surface motion on a small scale or simultaneously observing the temperature distribution and the motion of a thermal structure seem to be the most common use of thermal imaging for measuring flow rates.

At most infrared wavelengths, very thin volumes of water are opaque (McAlister, 1964). Thus, when a thermal camera is used to detect the temperature of a water body, the temperature of only a very thin volume of the water at its surface is being measured. Figure 2.1, from McAlister (1964) shows the absorption curve for 7.5 to 14 micron infrared light in water. McAlister (1964) showed that for light wavelengths of 7.5 to 14 microns, water is optically opaque for thicknesses of 0.02 mm or greater. This is the range of wavelengths detected by the infrared camera used in this study, confirming that what the camera measures is essentially the water surface temperature. This is important,

because it means that when thermal imagery is used to compute temperature gradients or velocity distributions, they are being measured at the water surface.

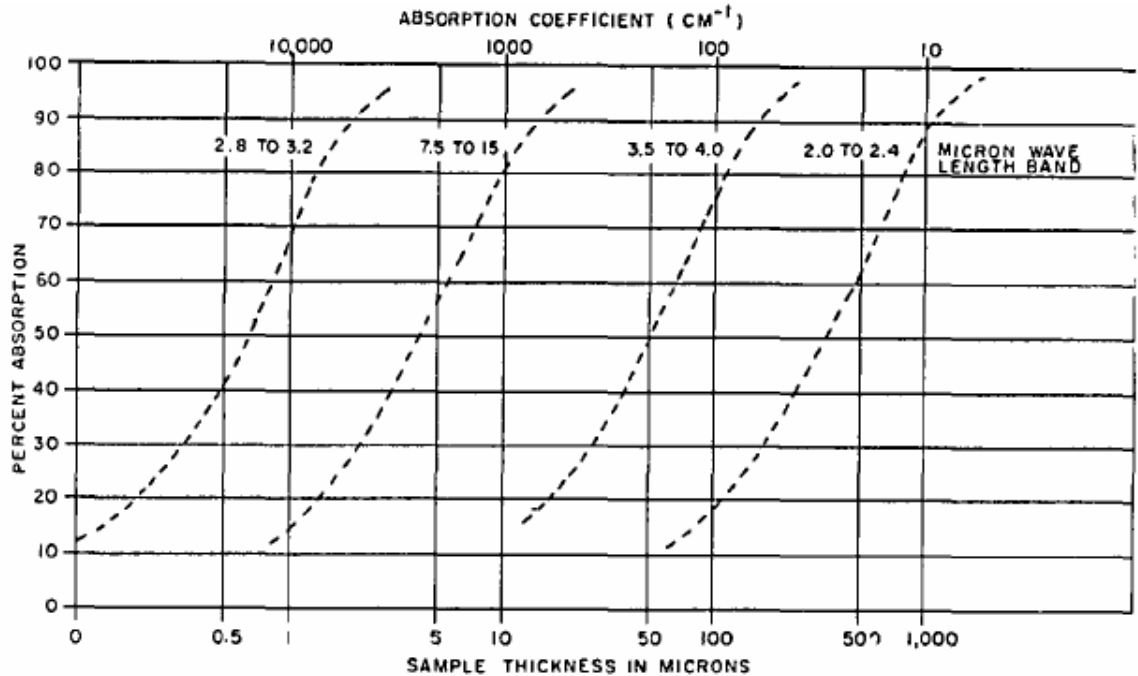


Figure 2.1 Absorption coefficient of water for selected ranges of infrared light (after McAlister, 1964).

In field applications, the flow must often be viewed from the side or at an angle. Except for at large viewing angles, the emissivity of water is quite high for the wavelengths of light (7.5 to 13 microns) that are measured in this thesis. Figure 2.2 shows how the emissivity of infrared light varies with wavelength and viewing angle. Even at a fairly large viewing angle of 80 degrees, the emissivity of the water is still quite high. However, if the viewing angle increases more, the emissivity drops off rapidly. In some cases the flow is being viewed from an elevation of only about 10 meters above the flow. In these cases, it can be expected that the emissivity will drop off rapidly as the viewing distance increases beyond 50 to 100 meters.

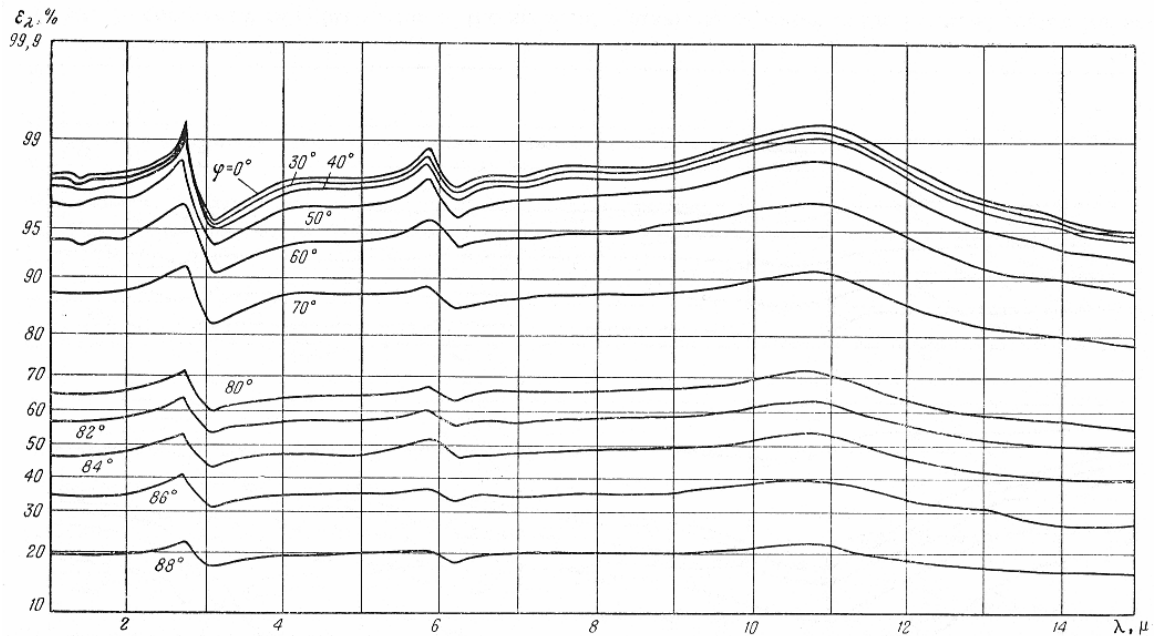


Figure 2.2 Spectral emissivity of water in the infrared region for selected angles of view. Probability scale (after Bramson, 1968)

One of the first studies on the use of thermal imagery to track surface velocity was done by Meadows et al. (1991). They used a 10 Watt CO₂ laser operating at a wavelength of 10.6 microns to heat a water surface over an array of points. The heated points were then tracked in a Lagrangian fashion using thermal imaging cameras. The laser was capable of heating up to 40 points per second on the flow surface to a temperature that was approximately 0.75 degrees above ambient. The thermal imagers were able to resolve the heated patterns for approximately 0.75 seconds before dissipation of the heat had diminished the temperature signature too much to be identified.

Other early users of thermal imaging for flow measurement include Jähne and Haußecker (1998) demonstrating the use of thermal imagery for investigating exchange of gases at the air-water interface. Their use of the technology used the technique called the controlled flux technique that used a known controllable flux density tracer applied to the

water surface. By using a CO₂ laser to heat up a spot on the water's surface, an IR camera can be used to track the spot to observe heat dispersion over time. It was found that the transfer velocities being measured were consistent with previous measurements by other authors.

Another form of thermal velocity tracking of large-scale structures was done by Hetsroni, Kowalewski, Hu, and Mosyak (2001). The method used a thin foil technique to observe turbulent flow structures on the wall caused by interactions between the flow and the wall. The flow was turbulent and shallow with a 37 mm flow depth, and with this setup the camera could be placed below the flow to observe the heat footprint of turbulent structure movements on the foil. A tracking algorithm was then able to accurately calculate the varying velocity magnitudes.

Zhang and Harrison (2004) used infrared imaging techniques to observe temperature and velocity distributions of a wind-driven water surface. The surface velocities were determined by movement of structures on the surface of the water. From these velocities, it was found that the mean wind drift is approximately 25% less than the widely cited measurements of 55% of the shear velocity caused by the wind on the water surface. It was also shown that the probability distribution function of the standardized water surface temperature does not vary significantly with wind speed.

Jessup and Phadnis (2005) investigated geometric properties and velocities associated with microscale breaking waves in a wind-wave tank. Velocities of the wave crests were

determined using 2 methods, an image-PIV algorithm computing the pixel displacement between two sequential images using a localized spatial cross correlation technique and a crest-PIV method comparing crest movement between sequential images. The sample frame rate that was used between images was 60 Hz so there would be enough separation between the waves in the two images. It was found that the crest-PIV method produced inaccurate vectors on the edge of the crests. The image-PIV method provided more accurate vectors, though there was a tendency to produce magnitude estimates that were biased low.

2.3 Techniques Used

Calculation of the surface velocity was done with the help of the minimum quadratic difference (MQD) formulation from Gui and Merzkirch et al. (2000). The MQD method uses the following function.

$$D(m, n) = \frac{1}{M \cdot N} \sum_{i=0}^{M-1} \sum_{j=0}^{N-1} [g(i, j) - g'(i + m, j + n)]^2 \quad (2.1)$$

When D is at its minimum value it yields the optimum correlation between two two-dimensional arrays. In the present case, the optimum correlation is also the displacement of the water surface between the two compared images. This method was used since it gave better results than other correlation methods tried such as a cross-correlation based on a Fourier Transform. The Fourier transform, commonly used to calculate correlations for PIV, was found to be inferior to the MQD formulation most likely because it lacked the ability to effectively handle continuous gradients of temperature on the water surface (as opposed to discrete particles found in typical PIV applications).

Images were rectified using a method described by Fujita et al. (1997, 1998). Fujita presented the video image transformation and used it on video taken of a flood in Japan, where the flood was too large to be covered by a conventional probe-type measurement method. Images were transformed from the distorted CRT coordinates (x,y) of the camera to the non-distorted physical coordinates (X,Y) of the water surface, and required at least four points for the transformation to work. Calculation of the two-dimensional velocity distribution of the water surface was calculated by using debris in the water for velocity tracers. The section being recorded was over an area where the profile was known, allowing the $1/7^{\text{th}}$ power law to be used to calculate the flow discharge. This method was accurate within an error of 3% compared to a stage-discharge curve at the same section. The $1/7^{\text{th}}$ power law has been used in many situations to calculate discharges from surface velocity measurements (e.g., Ettema et al, 1997; Admiraal et al, 2004). The power law has been shown to work well for calculating total discharge for applications in which the ratio of channel width to channel depth is large, and when channel depth does not change rapidly with spatial location. This is true of many natural and man-made water bodies, making the power law a simple, but powerful discharge calculation tool.

2.4 Particle Image Velocimetry (PIV) Methods

Digitally recorded images were used by Willert and Gharib (1991) to perform PIV techniques. They were among the first to apply the contemporary method of interrogating digital images to obtain detailed velocity information. The digital images

allowed them to avoid processing film for PIV measurements, and to directly process the images. This made the PIV method much easier to perform. The images were recorded at 30 Hz or slower, limiting the speed of the flow being recorded. It was found that the digital image method could be implemented in place of the previous method and give accurate results. It was stated that the real strength of using the digital images was that the images can be captured, viewed, and processed without delay. The only disadvantages to the technique noted were due to a lower resolution that would eventually improve with higher resolution digital cameras.

Accuracy of PIV measurements was discussed by Cowen (2000), he identified some ways to lessen apparent turbulence and velocities. Use of a 64x64 pixel interrogation area was able to keep displacement determination errors to a minimum. Also, the optimal pixel size for tracking discrete objects to minimize error was found to be 2 pixels. Tracers with fewer than two pixels made it impossible to obtain particle position with subpixel resolution. It was also noted that care needs to be taken to only view the surface particles and not the ones below the wave being tracked.

A statistical investigation of errors in PIV was provided by Guezennec and Kiritsis (1990). Synthesized images were used to insure that actual displacements would be known exactly, because two-dimensional velocities calculated with real images could not be exactly determined. It was found that the most important factor for accuracy was the ability to separate the particle from the background, selecting a proper threshold and getting enough contrast compared to the background noise was important. This is

definitely an issue for thermal velocimetry when background noise is at the same level as measurements of thermal variations, and camera sensitivity is a key factor.

Chapter 3. Instrumentation

3.1 Introduction

The objective of this research project is to develop a method to measure the surface velocities of water bodies using thermal imaging. Several pieces of equipment are used to gather data sets that can be combined to calculate water surface velocities.

The IR camera collects consecutive thermal images of the target water body. These images can be processed to calculate water velocities, but in order to do so, the scale and orientation of the images must be determined. Thus, control points must be established for all of the thermal images. Control points are used to determine scale and to modify the image using a matrix transformation, especially in the field, where the angle of the camera relative to the water surface is oblique. In the lab, known distances and calibration grids are used to determine control points. In the field, control points are determined using a total station. Once the images are scaled and corrected, two sequential images can be compared to each other to measure surface velocities.

To calculate discharge, the depth profile of the channel must also be known. For field measurements, depth profiles collected from the Nebraska Public Power District (NPPD) are used. One set of Acoustic Doppler Current Profiler (ADCP) data is also available, from which depth profiles can be determined. In laboratory measurements, profiles of the laboratory channels are known, but depths are measured with point gages.

Finally, for comparison purposes, discharges were independently measured in both the laboratory and the field. In the laboratory, a v-notch weir was used to measure discharge. In the field discharges were provided by NPPD who had rating curves and Sontek Argonaut measurements. In addition, some of the field data were supplemented with Acoustic Doppler Current Profiler measurements.

In this chapter, the instrumentation identified in the previous paragraph is described in more detail.

3.2 Infrared Camera System

The infrared camera system is used to gather thermal images followed by processing the images. The IR camera system consists of a FLIR Systems ThermaCAM camera and PC software designed to process the IR camera files. The infrared camera used was a FLIR Systems ThermaCAM S65HSV. Technical specifications for the ThermaCAM S65HSV from the technical specifications paper are shown in Table 3.1, and the camera is pictured in Figure 3.1. For the purposes of this project, the most important parameter in Table 3.1 is probably the sensitivity. In order to track thermal structures with very small temperature gradients, high sensitivity is necessary. The absolute temperature of the water surface is not as important as the motion of the surface structures, and surface temperatures do not have to be accurate as long as error in the measurements is bias error and not random error.

Some key features of the IR camera are that images can be stored on the camera, a memory card, or directly to a PC. It also has a 4 inch display with controls connected to the IR camera through a cable that allow for easier viewing and control of the camera. The camera could be powered from an outlet during laboratory testing or by batteries in the field.

Table 3.1 ThermaCam S65HSV Technical Specifications (FLIR Systems, 2006)

Description	Values
Spectral range	7.5 to 13 μm
Thermal sensitivity	50mK at 30° C
Accuracy (% of reading)	$\pm 2^\circ \text{C}$ or $\pm 2\%$
Emissivity corrections	Variable from 0.1 to 1.0 or selected from listings in pre-defined material list
Field of view/min focus distance	20° x 15° / 0.3 m
Temperature ranges	-40° C to +120° C 0° C to +250° C +100° C to +500° C +250° C to +1500° C
Detector type	Array
Cooling	Uncooled



Figure 3.1 ThermoCAM S65HSV (www.flirthermography.com, 2009)

The camera can be used as a stand alone system, though the ThermoCAM software enhances the effectiveness and speed that data is able to be collected, viewed, and processed. The software used to extract image data from sequences collected with the camera is FLIR Systems ThermoCAM Researcher Professional 2.8 SR-3 running on a PC. In addition to recording images from the IR camera, the software is able to control the IR camera through a FireWire cable connection, allowing the camera to be remotely controlled with a PC. The software also allows for viewing and playback of all collected images, making it possible to change the center and span of the viewable temperature distribution without changing image data. This allows the viewer to more easily see the movement of the water surface if temperature gradients on the surface are small. The software can also export images into formats that can be used for other purposes, such as the flir public format (.fpf) for processing and .avi video files. An example image of the ThermoCAM GUI is provided in Figure 3.2.

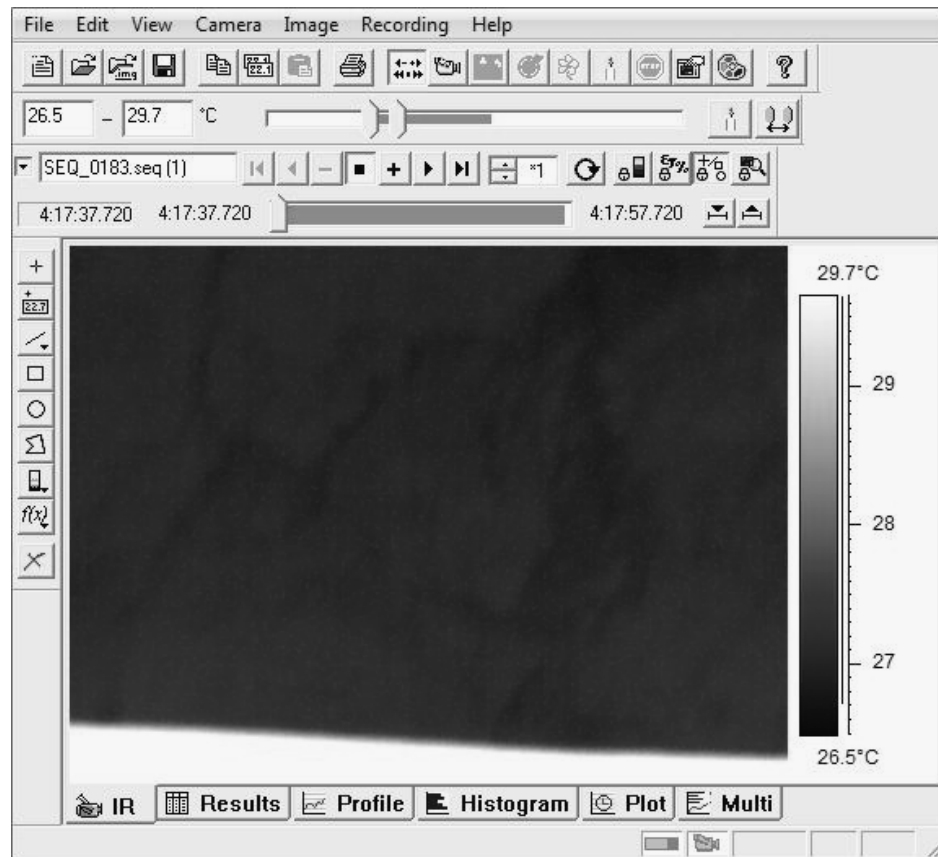


Figure 3.2 An example of ThermaCAM software GUI.

For the lab experiments the IR camera was mounted above the water channel and connected to a PC running the ThermaCAM software. This configuration allowed us to view what the IR camera was imaging, and to trigger image acquisition when the seeded water was entering the viewing field. The laboratory data was recorded directly to the PC, making it possible to review the data soon after it was collected.

For the experiments performed in the field the IR camera was either mounted to a bracket connected to the top of the total station or to a tripod immediately adjacent to the total station. The image data were recorded to a memory card and then transferred to a laptop after recording for the day was completed.

3.3 Total Station

The total station is survey equipment that was used to determine the exact position of reference points with respect to the position of the thermal imaging camera. The total station provided vertical angles, horizontal angles, and distances from the camera for each of the control points. The control points could then be used to correct oblique images so that true velocities could be determined from thermal images. The total station used to collect position reference point data in the field was a Sokkia Set 5A total station.

A prism was moved around to each of the control points that were chosen to correct the oblique images. The total station was used to measure vertical and horizontal angles to the target prism by aligning the crosshairs in the eye piece of the station with the crosshairs on the target prism. It measured distance to the prism by sending an infrared beam to the prism placed at the target location. The infrared beam was reflected back to the total station, and the total station measured the time the beam took to travel to and from the prism, using the travel time to determine the distance to the prism. The prism worked as a corner cube reflector so that the infrared pulse was sent directly back to the total station even if the prism was not exactly aligned with the infrared signal from the total station. The total station used the direct distance along with the vertical angle necessary to target the prism to calculate the horizontal and vertical distance of each position reference point in relation to the total station. These measurements, along with

the horizontal angle gave a precise location of each position reference point in relation to the total station.

The total station has an angular accuracy of 10" with a distance range of 800 m under average conditions. There is also a standard deviation of $\pm(5\text{mm} + 5\text{ppm} \times D)$ where ppm is an atmospheric correction factor for temperature and pressure and D is the distance to the target prism. Atmospheric corrections were not made since the distances measured with the total station were less than 200 m, a distance guideline for corrections stated in the Sokkia Set5/Set5S Electronic Total Station Operator's Manual. An image of the total station is provided in Figure 3.3.



Figure 3.3 Sokkia total station

The total station was mounted on a tripod to allow the total station to be stabilized and leveled prior to each of the field measurements. For some field tests, the handle of the

total station was removed and the handle mounts were used as a base for the IR camera (i.e., the IR camera was mounted directly on the total station).

3.4 Acoustic Doppler Velocimeter

An Acoustic Doppler Velocimeter (ADV) gathers three-dimensional velocity measurements for measuring the velocity profile in a channel. The ADV used for our experiments was a SonTek 50 Hz MicroADV with a 16 MHz probe. The ADV is a single point three-dimensional Doppler current meter. Technical Specifications for the ADV system are given in Table 3.2. The ADV system consists of the ADV probe that is connected to a submersible conditioning module, that is then connected to a splash proof digital signal processor via a 10-meter cord. The digital signal processor is then connected to a PC via a serial cable. A photo of the entire ADV system is provided in Figure 3.2 and a close up of the probe showing the functionality is provided in Figure 3.3.

Table 3.2 ADV Technical Specifications (SonTek Manual 1997)

Description	Values
Accuracy	1% of measured velocity
Resolution	0.01 cm/s
Sampling rate	0.1 to 50 Hz
Sampling volume	0.9 cm ³
Distance to sampling volume	5 cm
Possible velocity ranges	3, 10, 30, 100, 250 cm/s

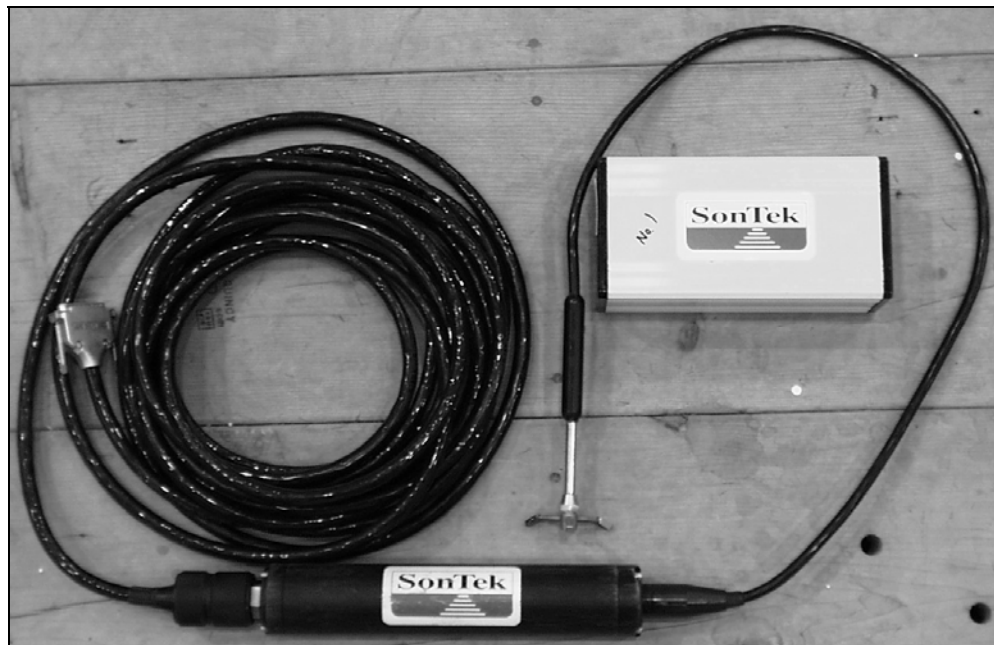


Figure 3.4 ADV system with the probe in center, the conditioning module on bottom and the signal processor on top.

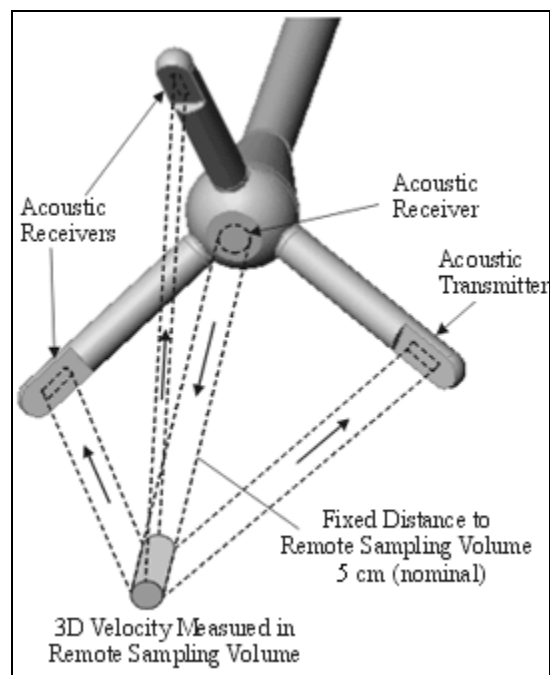


Figure 3.5 Close-up of the ADV probe. (www.sontek.com, 2009)

The ADV was mounted on a point gauge and placed in the large flume so that the end of the probe would be in the center of the channel facing the side of the tank. It was

mounted on the point gauge so the depth of the probe was known, and oriented sideways so that the probe could measure both close to the surface and close to the bed of the flow.

3.5 Point Gages

Point gages were used to measure depths in the laboratory channels. Two point gages were used in the small flume, one at 30.5 cm (1 ft) from the entrance of the channel and the other at 711 cm (23 ft, 4 in) from the entrance. Three point gages were used in the large flume, the gages were located at 30.5 cm (1 ft), 335 cm (11 ft) and 686 cm (22 ft, 6 in) from the entrance of the channel. The sensitivity of the point gages used in the experiments was one hundredth of a centimeter. The accuracy of the point gages was estimated to be about three hundredths of a centimeter.

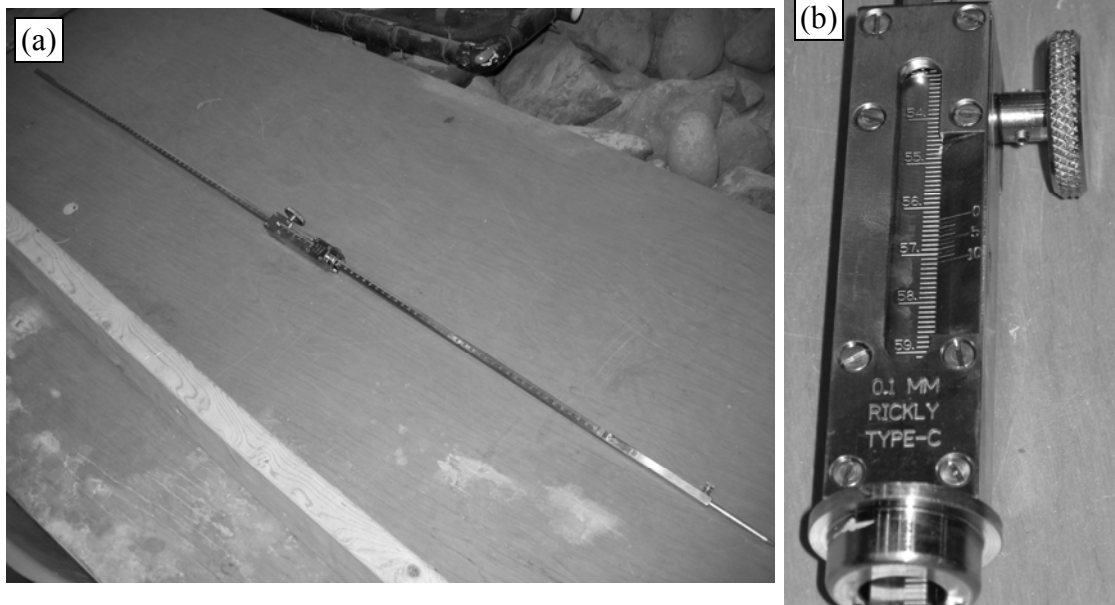


Figure 3.6 (a) Example of a point gage used. (b) Close up of point gage.

3.6 V-notch Weir

A 30 degree v-notch weir was used to measure the discharge in the laboratory. The weir is located at the end of a return channel into which the testing channels drain. The weir is shown in Figure 3.7. The height of the water above the crest of the weir (H) was measured using a point gage similar to the one in Figure 3.6. The equation typically used for calculating the flow rate of a V-notch weir is:

$$Q = \frac{8}{15} C_D \sqrt{2g} H^{\frac{5}{2}} \tan \frac{\theta}{2} \quad (3.1)$$

Where Q is the discharge in m³/s, C_D is the discharge coefficient of the weir, g is the acceleration of gravity, H is the height of the water above the weir crest in the V-notch, and θ is the angle of the notch.

A calibration of the weir in the lab was performed by Clark (2009) to provide more accurate flow rate comparisons. It was shown that the discharge coefficient for the weir in the lab was 0.686, which is higher than that of a standard weir. This is likely caused by the reduced flow area and high approach velocity upstream of the weir.



Figure 3.7 The V-Notch weir used to measure discharges in the lab.

3.7 Acoustic Doppler Current Profiler

An Acoustic Doppler Current Profiler (ADCP) was used to measure depth profiles and discharges in field experiments. The depth profiles were used to increase the accuracy of discharge rate calculations at the locations where velocity was measured, and to give more information about the profile of the canal bottom than could be provided from the single transect provided by the NPPD. Along with providing a more detailed profile, the ADCP also provided discharge information for compare with thermal imagery results.

The ADCP used for field measurements was a Workhorse Rio Grande 1200 kHz ADCP from RD Instruments and is shown in Figure 3.8. The ADCP has four independent beams that measure velocities in three dimensions with a redundant beam for an error

check. As is stated in Schemper (2007) ADCP Mode 1 was the best operating mode for the present canal measurements due to the speed and shallowness of the flow.

The ADCP was mounted to a raft that was pulled across the canal with a set of ropes, with the raft remaining mostly parallel to the flow. A container on the raft held the power supply for the ADCP, the battery, and the laptop to which the ADCP output data was recorded.



Figure 3.8 Workhorse Rio Grande 1200 kHz ADCP

Each ensemble of data recorded by the ADCP contains the position of the ADCP, a velocity profile, and the depth. As the ADCP is pulled across the channel, it records many ensembles of data to a file on the computer.

Chapter 4. Data Collection and Experimental Procedure

4.1 Data Collection Overview

Data were collected in three locations. Initial tests were done in a 70-cm wide, 10-m long flume that allowed for development of basic surface velocity tracking techniques. A second set of tests was completed in a 240-cm wide, 7-m long flume to develop camera angle correction and to examine artificial seeding with a laser. Finally, data were collected in the field where final experimental methods could be assessed. Additional information is provided about other field sites that were examined to reveal some of the considerations and complications associated with thermal imaging measurements.

4.2 70-cm Flume Test

The initial tests performed in the 70-cm flume were done to get information and data about the plausibility of using the IR camera for tracking surface velocities of water. Additional tests in the 70-cm flume helped develop the basic techniques used for tracking water surface velocity. A diagram of the 70-cm flume experimental setup is given below in Figure 4.1. The exact dimensions of the 70-cm flume were 70 cm (28 in) wide and 9.75 m (32 ft) long with a maximum depth of 46 cm (1.5 ft). The maximum flow rate in the flume was approximately 71 L/s (2.5 ft³/s). The forebay upstream of the 70-cm channel was 2.29 m (7.5 ft) long and contained a diffuser and filter to condition the flow and to reduce waves in the channel.

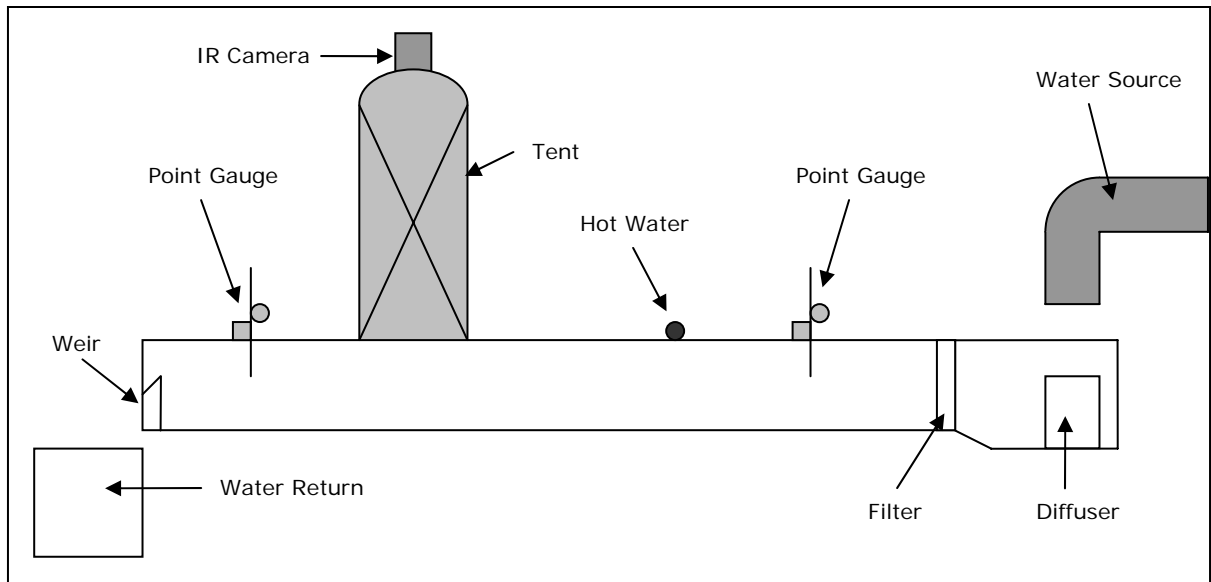


Figure 4.1 Small flume experimental setup

The IR camera was mounted on a cart that was rolled into place on an I-beam above the flume. The IR camera was mounted perpendicular to the water surface so that images collected with the camera were not oblique. The IR camera was mounted 7.32 m (24 ft) downstream of the channel inlet and was pointed straight down with the lens 2.69 m (8.83 ft) above the bed of the flume. A canvas tent surrounded the viewing region of the IR camera from the top of the camera to the tops of the walls of the flume. The canvas tent was installed to prevent reflections from laboratory lights and other sources of infrared radiation from interfering with flow measurements. Two point gauges were installed to make average depth measurements: one was 0.31 m (1 ft) downstream of the inlet of the channel and the other was 7.11 m (23.3 ft) downstream of the inlet. When hot water was introduced into the stream as seeding material, it was introduced 1.27 m (4.17 ft) downstream of the inlet of the channel. The flow rate in the channel was measured using the 30-degree (total angle) V-notch weir installed in the return channel to the laboratory sump.

To reduce waves, break up the flow, and redistribute inflow more evenly in the forebay, a diffuser was placed in the forebay below the channel supply line. Also, for the three lowest flow rates a filter was installed at the entrance to the flume to further lessen surface waves. The filter was removed for the two largest flow rates since it interfered with flow development of these flows. The slope of the flume was negligible, and at the downstream end of the flume, a weir was used to control the depth in the flume.

Five flow rates were tested and for each flow rate five weir heights were used to control depth in the flume. The water surface was also seeded with hot water to provide higher water surface temperature gradients, making surface structures easier to identify with the IR camera. Each of the 25 flow rate/flow depth combinations was run four times, three times using various hot water seed rates and a fourth time with no seeding. Each run was then recorded at 3 different times to the PC, with each recording containing close to 13 seconds of infrared video for a total of approximately 400 images at 30 frames per second.

For the measurements associated with each flow rate and flow depth combination, the distance from the surface of the water to the IR camera was measured. For every run the temperatures of the supply water, seeding water, and air were recorded. The upstream and downstream average depth measurements were also collected. The final measurement made after every run, was the stage upstream of the V-notch weir so that flow rate could be determined. Complete test data for the sets of runs are shown in Table

A.1. Figure 4.2 shows a pair of images collected in the 70-cm flume for Test A. 3.1. The flow rate for this test is 0.417 cfs and the flow is seeded at a rate of 5 seconds on 30 seconds off. The images shown in Figure 4.2 have a separation time of 3 seconds to better illustrate the structure motion.

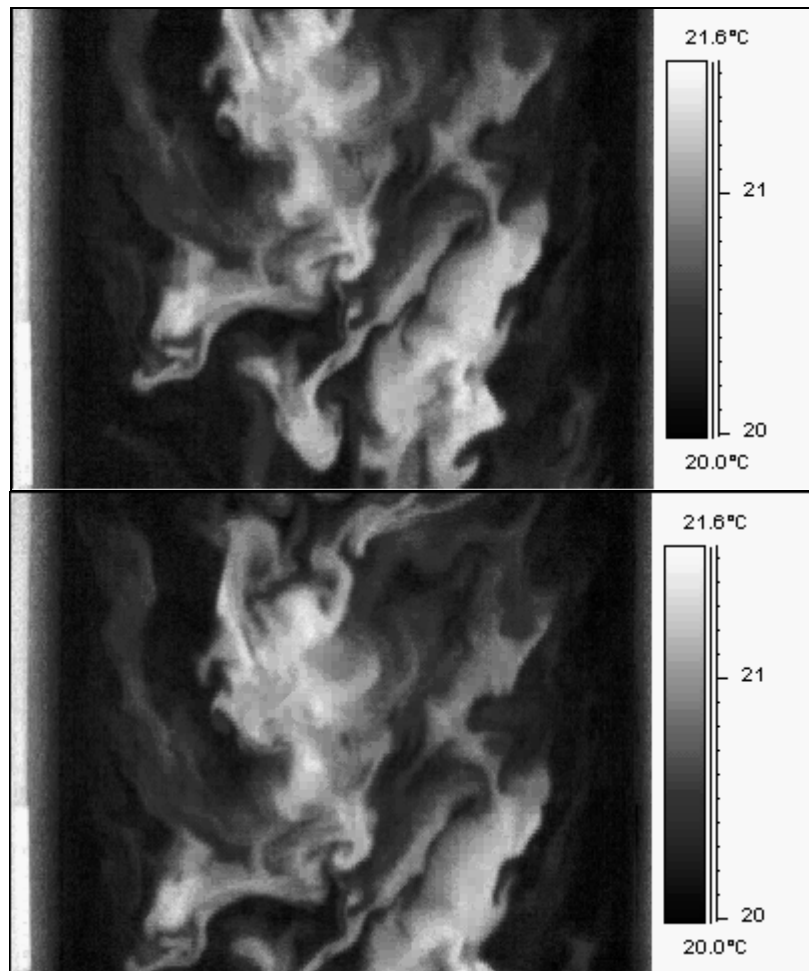


Figure 4.2 Thermal images showing seeded water moving through the measurement region for Test A. 3.1.

4.3 240-cm Flume Test

Additional testing in a 240-cm wide flume was used to investigate additional techniques for artificially seeding the flow and tracking the surface velocities of the water. This

time, the IR camera was placed so that it was not necessarily perpendicular to the water surface. This was done so that a method of correcting the image perspective distortion caused by viewing the water surface at an angle could be verified. To correct the image distortion, a grid with known dimensions was placed at the water surface so that it could be used to rectify the oblique images. The tests in the 240-cm wide flume were also seeded using a CO₂ laser instead of direct injection of hot water. This was done to reduce disturbance of the water surface. Furthermore, no tent was used to prevent reflections from contaminating water surface temperature measurements.

Figure 4.3 shows the experimental setup of the 240-cm wide flume. The exact dimensions of the 240-cm flume were 2.44 m (8 ft) wide by 7.16 m (23.5 ft) long with a maximum depth of 0.61 m (2 ft). The water entered the channel through a 2.62 m (8.58 ft) wide by 1.04 m (3.42 ft) long inlet bay and passed through a flow straightener before flowing into the channel. The diffuser and the flow straightener help to distribute water evenly across the width of the channel and also help to lesson waves in the channel. At the end of the channel was a 0.53 m (1.75 ft) long by 1.22 m (4 ft) wide weir trough to drain the water and adjust water depth in the flume.

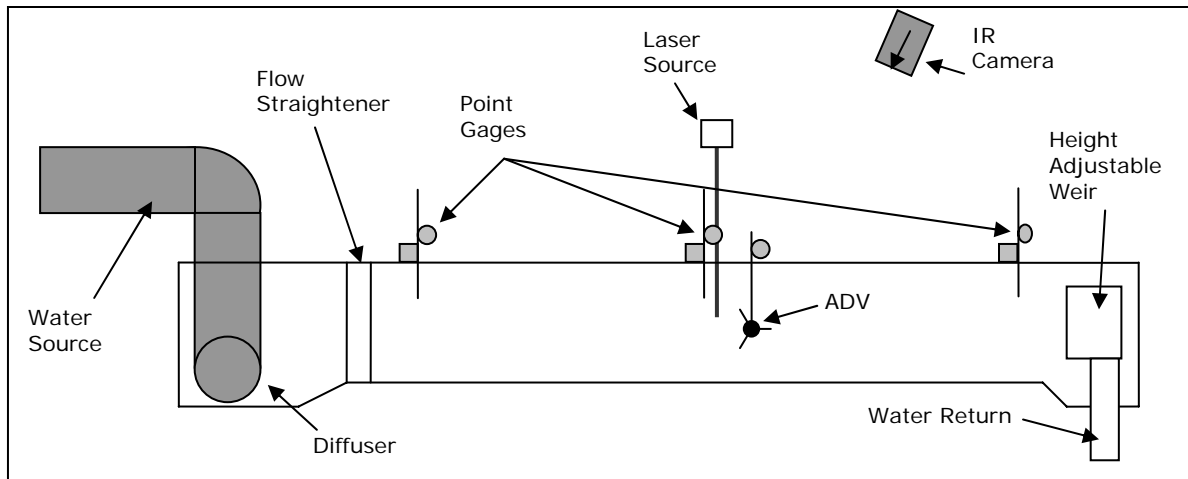


Figure 4.3 240-cm wide flume test setup

The IR camera was again placed on a rolling cart on an I-beam above the center of the flume to be rolled into various positions along the length of the I-beam. The camera was placed and angled so that the water would be heated just before entering the viewing region of the IR camera. Seeding of the surface water was done using a CO₂ laser that was reflected by a mirror to the center of the channel at 3.35 m (11 ft) from the channel entrance. Three point gauges were used to measure flow depth during the tests, the depth measurements were made at 0.31 m (1 ft), 3.35 m (11 ft) and 6.86 m (22.5 ft) from the channel entrance. Supplemental velocity measurements were made using an Acoustic Doppler Velocimeter (ADV) immediately downstream of the location where the water surface was heated by the laser. The ADV velocity measurements were made 3.46 m (11.33 ft) downstream of the channel entrance. The ADV was oriented sideways so that velocity could be measured near the bed and near the surface of the flow. Flow rate was again measured using the 30 degree V-notch weir located in the return channel to the laboratory sump.

Only one flow rate was investigated in the large flume. Before measurements were made, flow in the channel was set to an approximate depth of 0.18 m (0.58 ft). The flume was then emptied and a 20 cm by 20 cm (0.66 ft by 0.66 ft) grid was placed in the viewed region of the IR camera at the height of 0.18 m (0.58 ft). The grid was made using plastic fishing line attached to a steel frame. Two recordings were made with the grid, one using only the fishing line, and a second with metal staples placed at the grid intersections for easier identification of the intersection points within the IR images. Figure 4.4 shows a thermal image of the calibration grid with metal staples fastened to the intersections of the fishing line.

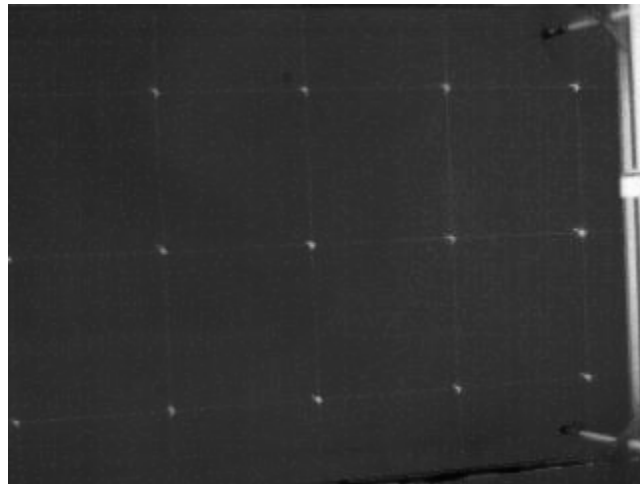


Figure 4.4 Thermal image of grid used to correct image distortion

The flow was restored in the channel to the same depth of 0.18 m (0.58 ft) that it was prior to calibration with the grid. Twelve runs were performed, three without laser seeding, three with the laser in a stationary position heating the water surface, three sweeping the laser across the water surface in a transverse oscillating pattern with an amplitude of 30 cm and a frequency of 0.5 Hz, and three sweeping the laser across the surface with an amplitude of 25 cm and a frequency of 1 Hz. The frequency of the laser

sweep was controlled with a galvanometer attached to the mirror reflecting the laser down to the water surface. The galvanometer was connected to a frequency generator. Finally, ten additional velocity measurements, each with a duration of 5 min, were made using the ADV. The velocity measurements were gathered at depths of 0.2 through 9.2 cm at increments of 1 cm. Depth measurements using the point gauges, bulk water temperature, and V-notch weir measurements were taken before and after the infrared measurements and also before and after the ADV velocity measurements. Test data are provided in Table B.1. Figures 4.5 through 4.8 show the region of the water surface as imaged by the IR camera (1) without seeding, (2) with the laser heating a fixed position of the water surface, (3) with the laser sweeping across a 30 cm section of the flow surface at a frequency of 0.5 Hz, and (4) with the laser sweeping across a 25 cm section of the flow surface at a frequency of 1.0 Hz, respectively.



Figure 4.5 Thermal image showing water surface in the 240-cm flume without seeding



Figure 4.6 Thermal image showing water flowing in the 240-cm flume with the laser pointed at a fixed surface position

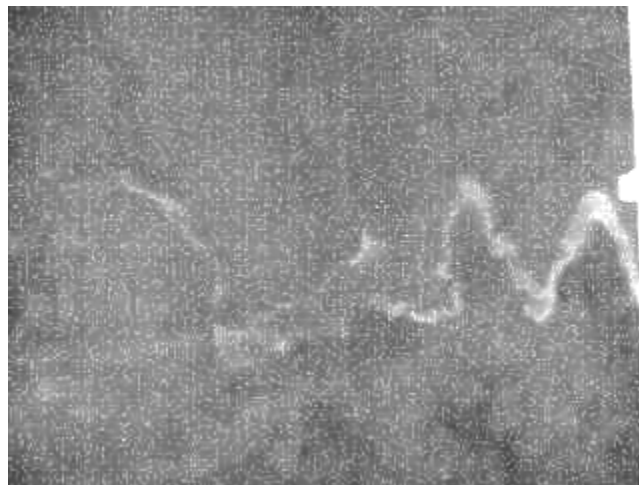


Figure 4.7 Thermal image showing water flowing in the 240-cm flume with the laser sweeping 30 cm across the surface at a frequency of 0.5 Hz.



Figure 4.8 Thermal image showing water flowing in the 240-cm flume with the laser sweeping 25 cm across the surface at a frequency of 1.0 Hz.

4.4 Transposition of Position Reference Points onto Large Water Surfaces

Position reference points, or control points, are used to rectify oblique images so that pixels in the rectified images have the same aspect ratio in both the x and y coordinate directions. Thus, an image viewed from the side can be rectified so that it appears as it would appear if viewed from directly above. Control points are points for which both the image coordinates (x, y) in pixels, and the object coordinates (X, Y) in meters or feet relative to a specified origin are known. The object coordinates can be determined with the camera location as the origin using a total station located at the same location as the camera. The corresponding image coordinates are found by identifying the location of the survey prism within the camera images. Control points should be scattered over the entire oblique image for best results when rectifying the image, and at least four control points are necessary to complete the rectification process. For large water bodies at oblique angles it can be difficult to identify adequate control points. In this section, a

method is described whereby control points can be transposed onto a water surface in order to obtain an adequate distribution of the points over the surface.

In ideal cases, real control points can be located entirely in the viewing area of the IR camera and viewed by the camera. These control points may be evenly spaced from each other in real space along the bank or across the water surface. The even distribution of control points in real space does not necessarily cause them to appear evenly distributed in the camera view.

For non-ideal cases the transposition of control points may be necessary to create virtual control points on the water surface. This is the case if the region of flow to be imaged by the thermal camera is inaccessible. The transposition of real control points, demonstrated in Figure 4.9, allows transposed control points to be overlain on the IR images used for the measurements. To create the transposed control points, the IR camera is mounted to the total station. Accessible, real control points are recorded on the edge of the water body with the IR camera and the horizontal angle of the total station is recorded. As long as vertical changes in the water surface elevation are small, the total station and the camera can be horizontally rotated, and virtual control points can be created at the same pixel locations in the measurement images as in the calibration images of the real control points. The object coordinates of the virtual control points are determined by doing a coordinate transformation of the real control points based on the angle through which the total station was rotated. By rotating the total station several times and recording the positions of the real control points in each new set of thermal images, several sets of

virtual control points can be created. These virtual control points can be used in the final horizontal rotation position of the camera to rectify the oblique images collected with the camera. In essence, what this method does is to create a transparency at each rotational angle where the position control points are marked. Then these transparencies are rotated about the axis of the total station and are laid over the final image set displaying all of the transposed control points. As long as the transposed control points are over the water surface and the water surface has negligible slope, it can be assumed that they are at the same height as the real control points, so it is then possible to calculate the real distances to the entire set of virtual control points.

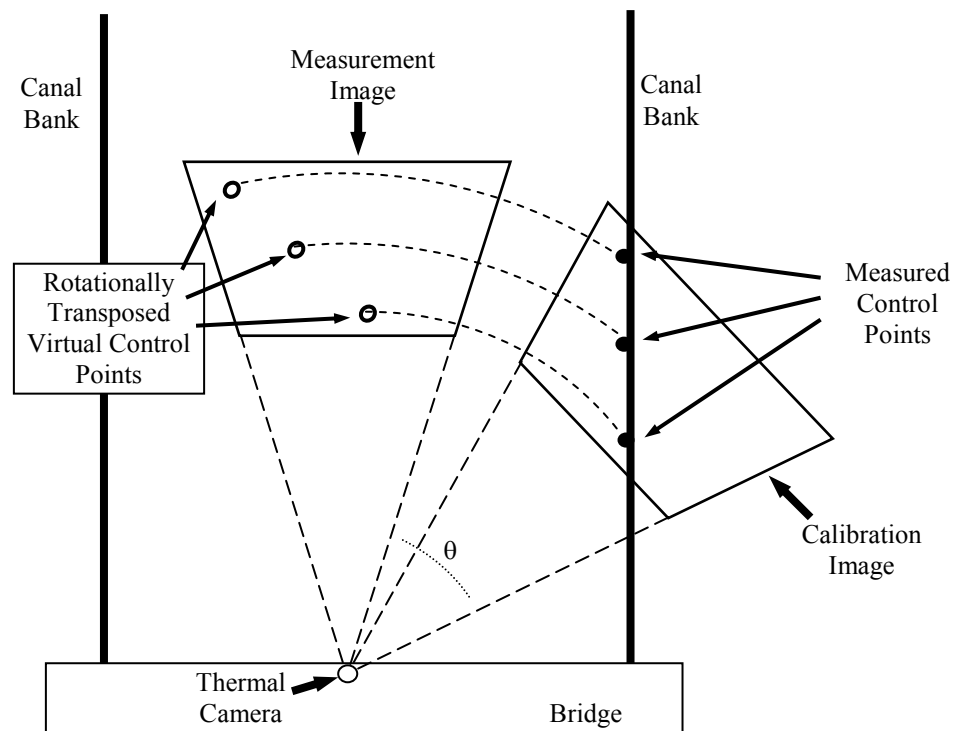


Figure 4.9 Rotational transposition of image calibration control points

4.5 The Irrigation Canal at Canaday Station

On August 4, 2008 thermal images of the Central Nebraska Public Power and Irrigation District Canal were collected near Canaday Power Plant in Lexington, Nebraska. An aerial photograph of the site is shown in Figure 4.10.



Figure 4.10 Aerial photograph of Canaday Station location with the hot water discharge near the bridge on the left, and a second bridge on the right. (Canaday Station outlet canal, maps.google.com, Aug, 2009)

At this location there was a hot water discharge on the north side of the canal. The discharge is the small channel that appears on the upper left side of the canal, near the road in Figure 4.10. The discharge emptied directly into the canal at a very high flow rate because it was the cooling water discharge of the nearby Canaday Steam Plant. Video sequences were gathered at several locations along the canal including (1) the discharge channel leading from the outfall to the canal, (2) a downstream view of the irrigation canal taken from the bridge next to the steam plant, (3) an upstream view of the

irrigation canal taken approximately one mile downstream of the road next to the steam plant. Images from each of these perspectives are shown in Figures 4.11 through 4.13, respectively.

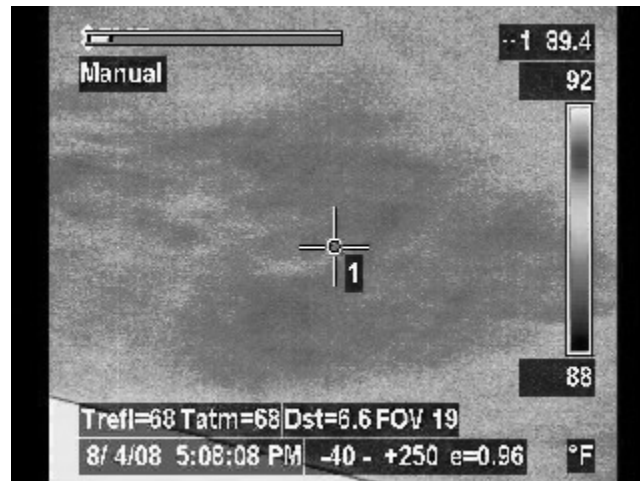


Figure 4.11 Discharge channel leading to the canal.



Figure 4.12 Downstream view of the irrigation canal.



Figure 4.13 Upstream view of irrigation canal.

None of the Canaday positions were selected as viable testing sites for the infrared flow measurement method. Flow in the outfall channel was too fast. The distance traveled by the water surface during the time between image frames would have been too great for standard image velocimetry techniques. Furthermore, the high level of air entrainment and the three-dimensionality of the flow in this channel did not make it conducive for discharge measurement.

Neither the upstream nor the downstream video sequences of the irrigation canal were adequate for testing purposes. The obliqueness of the images was too great to be accurately rectified because the bridge decks were only slightly higher than the water surface. In addition, the emissivity of a water surface is a strong function of angle at small viewing angles (Bramson, 1968), making it more difficult to identify temperature gradients when the camera was near the canal surface. The channel was approximately 100-m wide and unprotected from the wind. Waves on the water surface were significant due to strong winds, exacerbating problems associated with rectifying highly oblique

image sequences and resolving surface velocities. Hot water seeding of the flow was adequate, and the plume from the outfall was clearly visible, but flow measurement may only have been adequate if the camera was elevated using a boom or similar device.

4.6 Lake Ogallala

On August 5, 2008 data were collected at the Lake Ogallala water inlet, where it receives its water supply from the bottom of Lake McConaughy. The IR camera and total station were set up in a tourist observation area overlooking the Lake Ogallala inlet. Position reference points were identified to rectify the images so that velocities could be determined later. These position reference points were chosen along the bank of Lake Ogallala so that they could be easily spotted using the IR camera from the observation area. The coordinates of the chosen position reference points were then recorded using the total station and a handheld GPS unit. Locations of the camera and the position reference points are approximately identified in Figure 4.14.



Figure 4.14 Aerial image of the inlet of Lake Ogallala showing the location of the position reference points and camera. (Lake Ogallala inlet, maps.google.com, Aug, 2008)

Following the measurement of each position reference point, image sequences were taken with the IR camera. The images in Figures 4.15 through 4.17 show three camera orientations. The intent was to rectify images by mounting the camera to the total station

and transposing position reference points to the middle of the flow by simultaneously rotating the camera and the total station as described in Section 4.4.



Figure 4.15 Thermal image of the north shore of the Lake Ogallala Inlet



Figure 4.16 Thermal image of the center of the Lake Ogallala inlet



Figure 4.17 Thermal image of the south shore of the Lake Ogallala inlet

Because of temperature differences in the water coming from the hydropower plant, slight motion of the surface water could be seen in the corresponding video sequences. Unfortunately, the distances to the water surface were too great to accurately measure water surface velocities. The nearest position reference point was 1116 m from the camera so the best resolution possible would have been on the order of 1.5 m per pixel. This resolution was too poor to resolve most of the thermal gradients present on the water surface. A higher resolution camera or higher magnification might make flow measurement feasible at this site. A subsection of the imaged surface was not visible for processing because the hydropower plant structure and the outflow from the Howell-Bunger valve obstructed the view. It was interesting, however, that the interface between the warm water of Lake Ogallala and the cold inflow from Lake McConaughy was clearly visible (see Figure 4.16). Even though velocities were not readily measurable, at least the path of the inflow through the lake could be determined.

4.7 Sutherland Reservoir Cooling Pond Inflow Canal above Drop Structure

Three potential test sites were investigated in the vicinity of Sutherland Reservoir. The test sites are identified in Figure 4.18. The three potential test sites that were investigated include the inflow canal to the cooling pond near the drop structure, the cooling pond outlet into Sutherland Reservoir, and the Sutherland Reservoir outlet into the NPPD power canal. The three potential test sites will be discussed in turn, beginning in this section with the cooling pond inflow canal.



*Figure 4.18 Map locating the three sites considered at Sutherland Reservoir.
(Sutherland Reservoir, maps.google.com, Aug, 2009)*

Thermal images were taken of the Sutherland Reservoir cooling pond inflow above the drop structure on August 5, 2008. The inflow is a canal that carries the cooling water discharge of Gerald Gentleman Station to the cooling pond. At this location the canal goes over a drop structure to dissipate energy before entering the cooling pond. A video

image was taken of the canal upstream of the bridge that crosses above the drop structure and is shown in Figure 4.19.

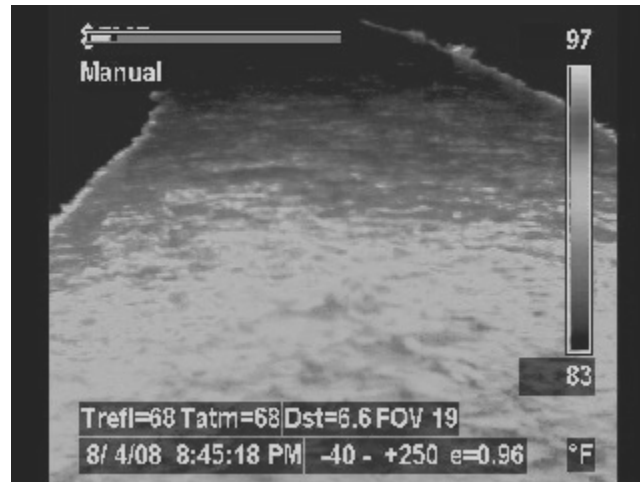


Figure 4.19 Inflow canal above the drop structure.

The cooling pond canal was not selected as a test sight due to waves being generated by the drop structure that traveled upstream. The wave crests appear as moving thermal structures on the IR camera due to the oblique viewing angle of the camera. These waves would interfere with the PIV tracking method used to identify actual gradient temperature structures in the canal. The temperature gradients in the canal were large enough to track, though the camera would have to be mounted on a boom over the water and more perpendicular to the flow to reduce the interference caused by the waves.

4.8 Sutherland Reservoir Cooling Pond Outlet

On August 5, 2008 thermal images were also taken of the cooling pond outlet going into the Sutherland Reservoir. These images show the warm water of the cooling pond dispersing in Sutherland Reservoir as shown in Figure 4.20.



Figure 4.20 Sutherland reservoir cooling pond outlet.

The temperature distribution of the cooling pond water going into Sutherland reservoir is very easy to see. This site did have large temperature gradients that could be easily seen, but the site was not chosen because the camera angle was very oblique and because there were large surface waves in the area of interest. Another deterrent from using this site were water busts that came out of the drainage gate at regular intervals; these would have interfered with PIV interrogation.

4.9 Sutherland Reservoir Outlet Canal

The outflow from Sutherland Reservoir exits into a canal between Sutherland Reservoir and Lake Maloney in North Platte. The canal is approximately 32 km (20 miles) in length and carries a maximum discharge on the order of $42.5 \text{ m}^3/\text{s}$ ($1500 \text{ ft}^3/\text{s}$) – the actual flow depends on irrigation demand. The 600-m long reach just downstream of the reservoir, as shown in Figure 4.21, provides a good test bed for using the infrared camera for several reasons: (1) A bridge located downstream of the reach is about 9.2 m above the canal and provides an excellent perspective, (2) The canal is excavated so that the

water surface is approximately 9 m below the surrounding land surface, providing good cover from wind effects – the sides of the canal also provide an excellent perspective, (3) A gauging station with an acoustic discharge measurement device is located at the upstream end of the reach, (4) discharge information is also available at the outlet of the canal 20 miles downstream, and (5) access to the canal and to the banks above the canal is very good, with access roads on both sides of the canal and on the tops of the banks above the canal.



Figure 4.21 Aerial photograph of the outlet from Sutherland Reservoir. (Sutherland Reservoir outlet canal, maps.google.com, Aug, 2008)

Three types of measurements were collected at this site. Two sets of images were taken from the bridge and a third set from the side of the canal. The first set of images from the bridge was collected with the camera pointed almost directly down towards the water surface, looking over the edge of the bridge. For these images, the imaged area was small and the camera had to be moved across the bridge, collecting image sequences at multiple positions across the bridge. The second set of images from the bridge are of the entire reach upstream of the bridge, with the camera located at the center of the bridge and the outlet of Sutherland Reservoir located at the top center of the collected images.

The third set of images was taken from above the bank of the canal, with the camera situated far enough from the water surface to capture the entire width of the canal. The tests at this site were attempted during two trips, one during 2008 and one during 2009.

Depth information and cross section information for the channel were provided by NPPD, but unfortunately discharge measurements in the canal were not available during 2008, though reasonable estimates could be made from discharges measured by NPPD 32 km downstream. During 2009, NPPD was able to provide discharges measured with a Sontek Argonaut acoustic sensor at the upstream end of the reach. In addition, an ADCP was used to directly measure discharges and depth profiles in the canal at several cross sections. Data for all three types of tests are provided in Appendix C.

4.9.1 Top view from the bridge above the canal

Images of the canal were taken from the bridge above the canal on August 5, 2008 with the camera pointed towards the water surface directly below the bridge. To measure the surface velocity of the entire width of the canal, the camera was moved across the bridge systematically, getting multiple sequences of images. The camera was moved horizontally two meters (6.58 ft) for each step, so that the edge of one set of images would overlap with the edge of the next set of images. The camera was located 10.8 m (35.33 ft) above the water, and the width of the canal under the bridge was 19.8 m (65 ft). Figure 4.22 is a thermal image of the water surface directly below the camera for the top-view tests.

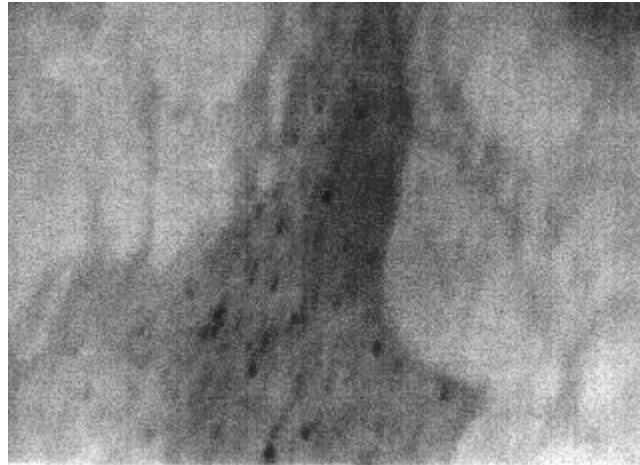


Figure 4.22 Sample image showing temperature differences in water below the bridge.

Distance measurement calibration was done by taking images of a marked pole on the edge of the canal. A sample image of the measurement calibration procedure is shown in Figure 4.23. In Figure 4.23, the edge of the canal and the pole at the water surface can easily be seen. A person holding a string connected to the two sides of the pole is visible in the upper left corner of the image. Since the length of the pole on the side of the canal is known, the pixel to distance ratio can be easily determined for the image. This ratio is the same for all images across the canal because the distance from the camera lens to the canal surface does not change from location to location.

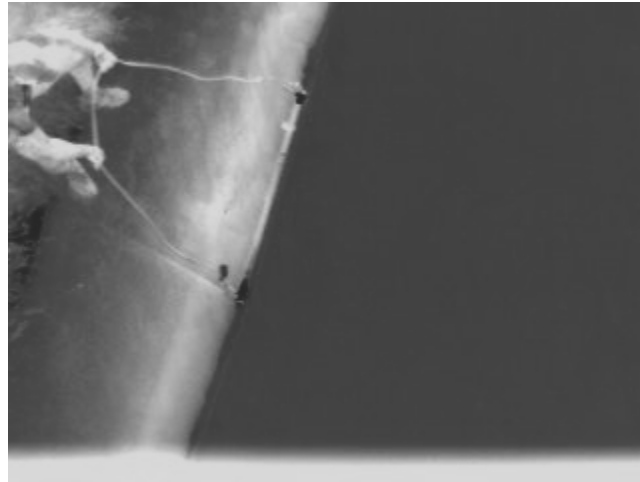


Figure 4.23 Thermal image showing measurement calibration marker

4.9.2 Upstream view of the canal

Viewing the canal from downstream provided an oblique perspective of most of the reach between the Sutherland Reservoir outlet and the bridge. Images of this view were taken on August 5, 2008 and also on July 21, 2009. In 2008, the transposition method described in section 4.4 was used to get position reference points across the canal surface. This was only partly successful because there was difficulty identifying the position reference points in the thermal images due to image resolution on the upstream end. In 2009, position reference points were identified on both sides of the canal for better rectification of the oblique images. To identify the coordinates of position reference points, the total station was used to mark the points along the bank of the canal. In 2008, three points were identified on one side of the canal and transposed, whereas in 2009 five points were identified on both sides of the canal without any transposition. Following calibration, images were taken with the camera pointed directly upstream with the reservoir outlet at the top center of the images. A sample image is given in Figure 4.24.

The width of the canal was measured to be 24.4m (80ft) across with a tape measure in 2008.

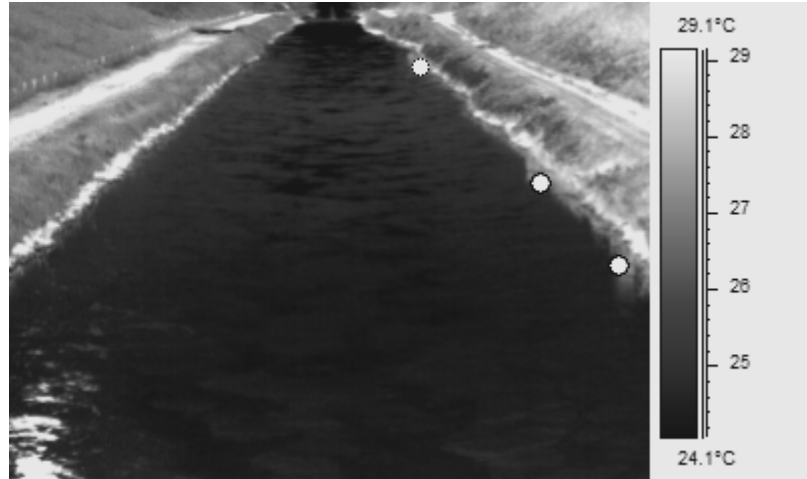


Figure 4.24 Thermal image of the NPPD Power Canal looking upstream from the bridge with the three position reference points used in 2008 marked

In 2009, survey points on both sides of the canal and GPS data provided a more accurate assessment of the channel geometry.

4.9.3 Side view of the canal

The side view of the canal provided another oblique perspective for calculating the flow in the canal. A sample image from the side of the canal is given in Figure 4.25 along with nine position reference points. In the side view images the canal flow is from right to left. In 2008, six position reference points were identified on the far bank in the images and three position reference points were identified on the near bank. The locations of all nine points were found using a total station. In 2009, five points were identified on the far bank and three were identified on the near bank. A GPS unit was also used to get the latitude and longitude of each point, but the GPS coordinates are less accurate than the total station data and were not used to rectify the images.

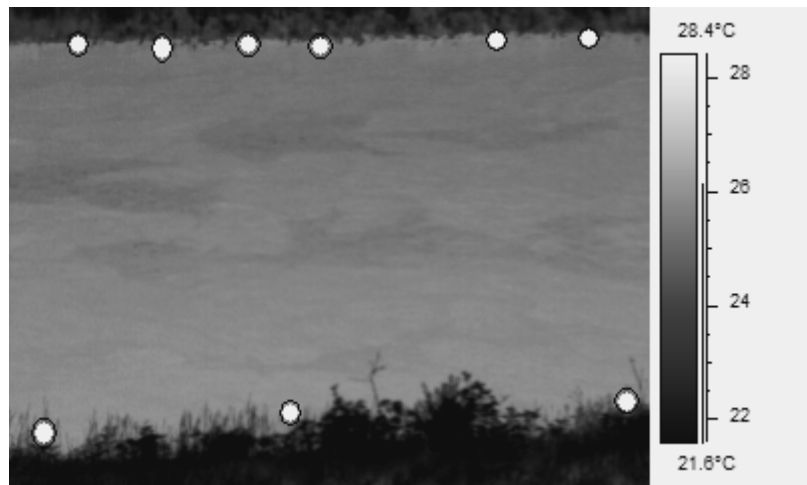


Figure 4.25 Thermal image taken from the side of the canal with nine position reference points marked

Calibration images were collected for each position reference point after the location of the position reference point was measured with the total station. Multiple sets of thermal image sequences were also taken while the position reference points were being recorded. The position reference points on the near side of the channel were measured with the prism held out over the water surface because the bank of the channel was steep enough so that the near edge of the channel was hidden by vegetation. Thus, velocity measurements could not be measured near the edge of the nearest bank, and had to be extrapolated. This region of the flow encompasses only a 2 m section near the bank, a relatively small section compared to the total width of about 25 m.

Chapter 5. Data Analysis Program and Process

5.1 Introduction

The data analysis was done using a program created by Dr. David Admiraal, called Flow Field Captor MD (FFCMD). The program allows for single images to be filtered to reduce noise, aligned to a master image to lessen unwanted camera movement and to be rectified to correct for the obliqueness. Once the images have been preprocessed, they can then be compared to each other to calculate the surface velocities of selected points in the images. The PIV processing segment of the FFCMD program is able to interrogate a single pair of images for a quick comparison and reference data or it can do batch processes to allow many images to be processed at once.

5.2 Image Processing Procedure

For each set of images, the same general image processing procedure is followed. Alignment of images is done first, followed by filtering and then oblique image correction; each of these processes is done only if necessary. Thermal images saved from the camera used the default file labeling system for storing the images as .FPF (Flir Public Format) files. An example of a filename is SEQ_02207.FPF, where 0220 is the number of the run and 7 is the image number in the series that can range from 1 to 600.

In some cases it was necessary to align images prior to processing because the camera occasionally moved due to wind or accidental movement of the camera while checking its status. The images were aligned by selecting non-moving features in the image (e.g. the canal banks) and using the program to check if they had shifted from image to image.

The program could detect the magnitude and direction of motion and could thus be used to realign images that had become misaligned. Though these misaligned images were not common, they had to be identified so that velocity data would not be contaminated. To signify that an image had been checked for alignment and if necessary realigned, the filename prefix “SEQ” was changed to “COR” (e.g., COR_02207.FPF) following realignment.

Images collected at oblique angles had to be rectified so that flow velocities could be accurately calculated. Images that were corrected for obliqueness were given the prefix “OBL” to indicate that they had been rectified (e.g., OBL_02207.FPF). Rectified images were sometimes filtered to see if filtering the images helped improve processing. Filtered images were not given a specific filename prefix, but were stored in different folders from unfiltered images. Finally the analyzed image data was stored in a file with a prefix of “ANA” like ANA_0220_99.txt where 0220 is still the number of the run but the 99 indicates the time separation of the images analyzed in milliseconds. All of the analyzed data were appended to one file for each variation of each run set, time separation and filtering.

5.3 Processing Procedure for Images Collected From the Side of the Canal

The side view of the canal was the most thoroughly tested set of all runs. To begin the processing of the side view images, all of the unprocessed SEQ images for all of the runs were aligned with the master image, SEQ_02241.FPF. The alignment procedure requires that the user first identify the region of the master image that is known to be stationary

(e.g. the banks of the canal). The image to be aligned is then shifted one pixel at a time in the x and y directions and the sum of the squares of the differences between all of the pixels in the interrogation region is calculated. This sum is calculated for every possible shift of the image being aligned according to x and y limits selected by the user. The minimum sum is then used to determine how much the image must be shifted to align it with the master image. If the limits set by the user are too small, the alignment procedure will be unsuccessful, but if the limits are large, the program requires a great deal of processing time. Thus, the limits were set as small as possible by trial and error before applying the alignment procedure to a batch of files. X and Y search limits for the alignment were both initially set to 10 pixels; if the calculated misalignment was near a search limit the limit was increased, conversely if the shift of the images was significantly less than the search limit the limit of the search was lowered to as little as 3 pixels more than the calculated misalignment. Once appropriate limits were set, all of the files belonging to a set were batch processed using the program as depicted in Figure 5.1.

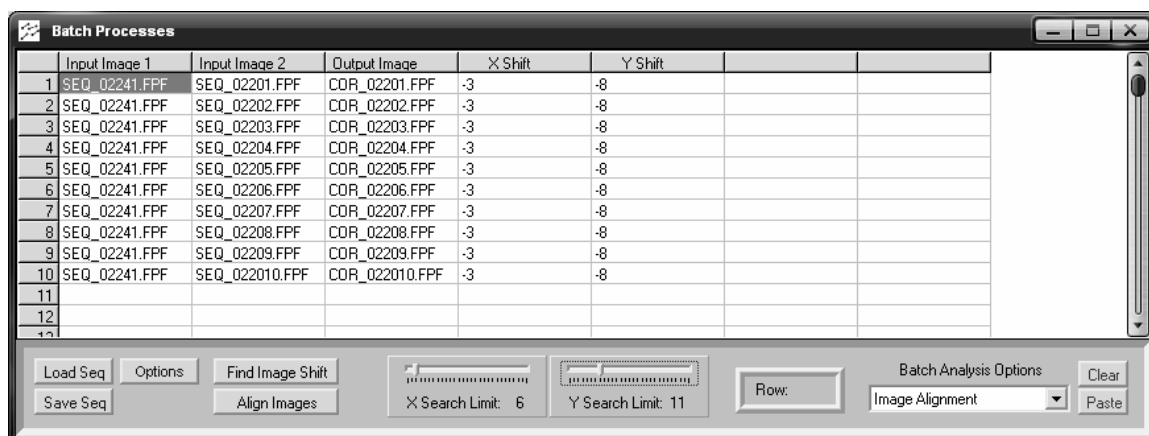


Figure 5.1 Sample of batch alignment dialog in FFCMD

Following image alignment the oblique images were rectified in two ways, creating two sets of rectified images. The first set was rectified without filtering the images. A second

set was rectified after first applying a nine pixel median filter to the images, making sure not to apply any image normalization so that the temperatures in the images remained accurate. To properly rectify the images it was necessary to provide the coordinates of at least four position reference points. For the images collected from the side view, eight or nine position reference points were used, depending on the data set. Selecting more points produced a slightly more accurate rectification process. To start the oblique image correction process the surveyed position reference points were entered into a table that calculates oblique correction coefficients as shown in Figure 5.2.

	X (m)	Y (m)	z (px)	v (px)	Rna (m)	EI (m)	dEI (m)	V Dq	V Mn	V Sc	H Dq	H Mn	H Sc	IH Dq	IH Mn	IH Sc	Cal. Image File
1	6.836511	-46.8464	301	13	47.7	10.7	0	102	38	50	280	51	20	270	0	0	
2	6.575533	-47.0022	254	15	47.46	10.7	0	102	42	10	277	57	50	270	0	0	
3	1.810422	-46.6548	168	17	46.69	10.7	0	102	55	30	272	13	20	270	0	0	
4	-0.66363	-46.8753	121	17	46.88	10.7	0	102	52	50	269	11	20	270	0	0	
5	-3.05770	-46.9304	71	17	47.03	10.7	0	102	48	30	266	16	20	270	0	0	
6	-5.34279	-47.2186	30	18	47.52	10.7	0	102	41	0	263	32	40	270	0	0	
7	-2.85239	-23.9406	36	210	24.11	10.7	0	114	7	40	263	12	20	270	0	0	
8	0.530631	-24.1041	157	201	24.11	10.7	0	113	58	0	271	15	40	270	0	0	
9	4.907305	-24.2586	311	198	24.75	10.7	0	113	34	30	281	26	10	270	0	0	
10																	
11																	
12																	
13																	
14																	
15																	
16																	
17																	
18																	
19																	
20																	
21																	
22																	
23																	
24																	

Figure 5.2 Oblique image correction coefficients table

The position reference points were then checked on a test image to see if they were in the correct positions. All position reference points required both object plane coordinates and image plane coordinates. The object plane coordinates were found by surveying the position reference points using a total station. A subroutine was written to convert the surveyed data points to Cartesian coordinates with the origin located at the total station.

Image plane coordinates were then found by identifying the surveyed points in the thermal images. If a position reference point was not in the correct position it could be moved interactively on the test image and the table automatically updated the new image coordinates of the position reference point. Figure 5.3 shows a sample test image with the locations of nine position reference points indicated by circles in the image.



Figure 5.3 Test image showing position reference point locations

Once the position reference points were in the correct position, an optimization was performed to find the coefficients necessary for image correction and the correction process could be applied to the oblique image to verify that all images would be corrected properly. Also the resolution and cropping of the rectified images were specified by the user prior to rectifying the images so that final images were reasonably sized and did not contain extraneous information at their edges (e.g., regions outside of the flow area),

making images smaller to reduce file size and processing time. All obliquely corrected images for the side view tests were cropped with an upper left pixel of $(x, y) = (10, 110)$ and a lower right pixel of $(x, y) = (690, 1122)$. An image of the dialog that allows the user to specify image resolution and cropping limits is provided in Figure 5.4 and a rectified oblique image is shown in Figure 5.5.

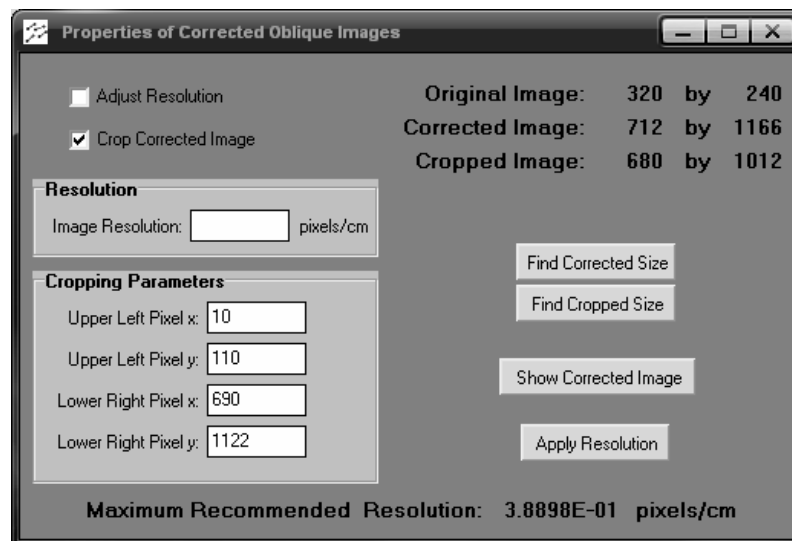


Figure 5.4 Dialog to specify image properties of rectified oblique images

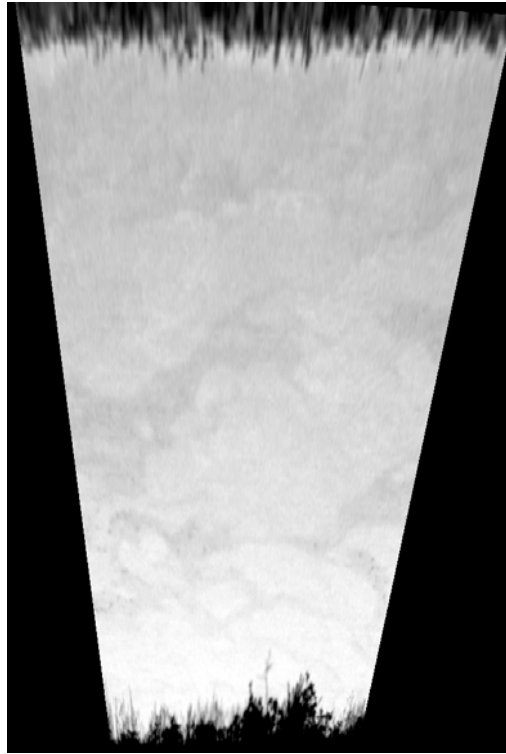


Figure 5.5 Oblique image of canal that has been rectified

After the position reference points were entered and the rectification coefficients were checked, the fixed pixel to distance ratio was determined. A dialog window in the program called “Distance and Timing” allowed the user to perform a “Distance Test”; in this procedure, the mouse was dragged across the corrected image from one position reference point to another, giving the pixel distance between the two points. Then the actual distance between the two position reference points, known from survey results, were entered into the program, and the program calculated the pixel to distance ratio (or the equivalent size of each pixel in the image in pixels per cm). The pixel to distance ratio determined for the side view images was 0.395 pixels per cm. Finally a batch process for each set of images was run to correct all of the oblique images in each file set. Again each set of images was corrected twice, once with a filter and once without a filter.

To turn on the filter there was a checkbox on the bottom of the batch process table. Four image filters were available in the program, but the nine point filter was always chosen if any filtering was performed. The images were also normalized based on the known temperature range of the flow, though this does not affect the flow measurement process. The batch table for oblique image correction is given in Figure 5.6 and an example of the difference between filtered and unfiltered images is shown in Figure 5.7. The filtered images are much smoother than the unfiltered images, the intent being to reduce the effects of background noise that might be present for individual pixels in the images.



Figure 5.6 Demonstration of batch processing table

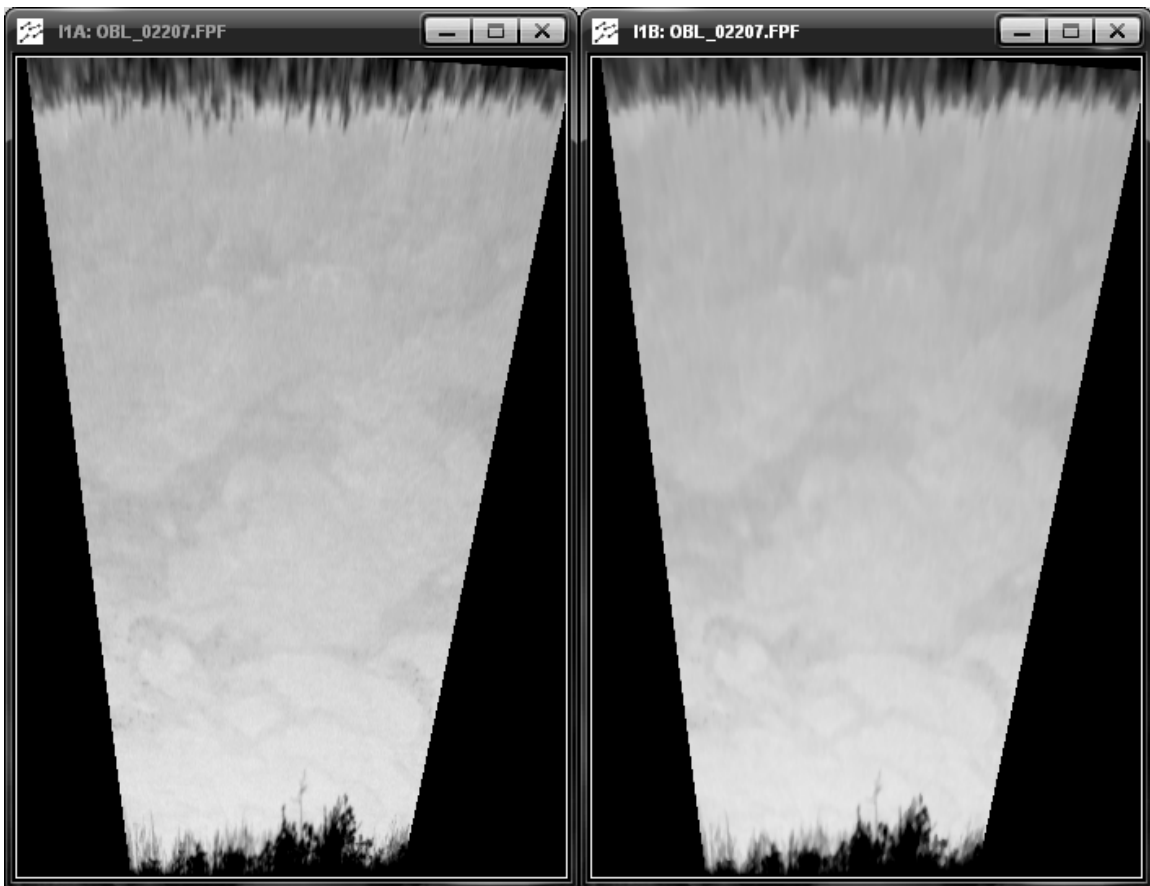


Figure 5.7 Rectified images, including unfiltered (left) and filtered (right) images

Finally the rectified images could be compared to each other to find the surface velocities. To begin this process the “PIV Results” table was opened and the coordinates of all of the points at which the surface velocity was to be measured were chosen. In the present case, three transects across the canal were used with either 10 or 12 points each, taking care not to allow the interrogation areas to overlap with the banks or image boundaries so that the results would not be biased. A minimum quadratic difference method (MQD) was applied in the program because it was found that Fast Fourier Transform (FFT) correlation methods did not work well for continuous data, the interrogation area was set to 128 by 128 pixels and the MQD Search Distance was set to

10 pixels. The separation time between images was specified for each pair of images in the batch process table. Figure 5.8 shows the batch process table for performing the particle image velocimetry.

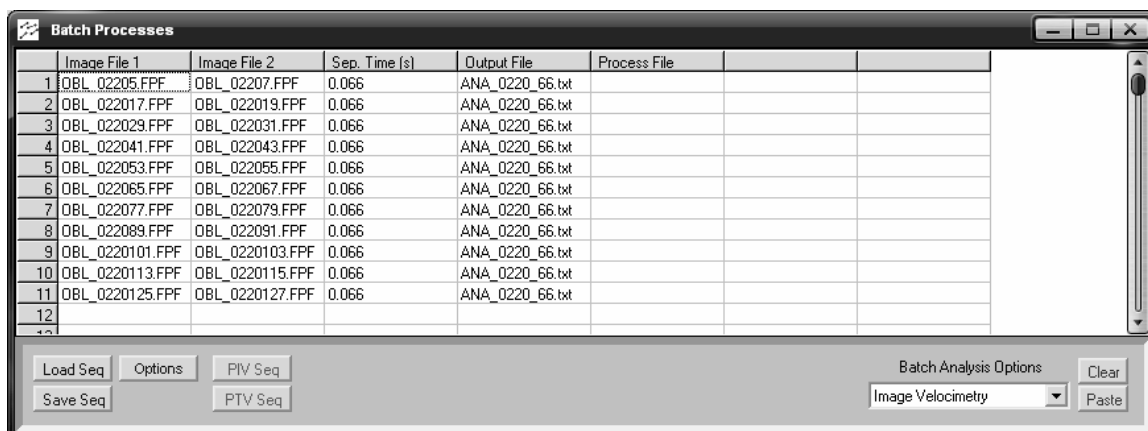


	Image File 1	Image File 2	Sep. Time (s)	Output File	Process File		
1	OBL_02205.FPF	OBL_02207.FPF	0.066	ANA_0220_66.txt			
2	OBL_022017.FPF	OBL_022019.FPF	0.066	ANA_0220_66.txt			
3	OBL_022029.FPF	OBL_022031.FPF	0.066	ANA_0220_66.txt			
4	OBL_022041.FPF	OBL_022043.FPF	0.066	ANA_0220_66.txt			
5	OBL_022053.FPF	OBL_022055.FPF	0.066	ANA_0220_66.txt			
6	OBL_022065.FPF	OBL_022067.FPF	0.066	ANA_0220_66.txt			
7	OBL_022077.FPF	OBL_022079.FPF	0.066	ANA_0220_66.txt			
8	OBL_022089.FPF	OBL_022091.FPF	0.066	ANA_0220_66.txt			
9	OBL_0220101.FPF	OBL_0220103.FPF	0.066	ANA_0220_66.txt			
10	OBL_0220113.FPF	OBL_0220115.FPF	0.066	ANA_0220_66.txt			
11	OBL_0220125.FPF	OBL_0220127.FPF	0.066	ANA_0220_66.txt			
12							
13							

The screenshot shows a software window titled "Batch Processes" with a table containing 13 rows of image pairs. The columns are labeled "Image File 1", "Image File 2", "Sep. Time (s)", "Output File", and "Process File". The first 11 rows contain data, with the remaining two rows (12 and 13) being empty. Below the table, there are several control buttons: "Load Seq", "Options", "PIV Seq", "Save Seq", and "PTV Seq". On the right side, there are "Batch Analysis Options" with a "Clear" button, and a dropdown menu currently set to "Image Velocimetry" with a "Paste" button.

Figure 5.8 Demonstration of Image Velocimetry batch table

5.4 Side View Processing Results, August 2008

For the August 2008 side view data, a total of six sets of test images were collected. Each set of test images was processed using oblique image correction with filters and without, and then 50 pairs of images were compared to each other from each set. This process was repeated four times: using pairs of images (1) from adjacent frames, (2) separated by one frame, (3) separated by two frames, and (4) separated by three frames. This procedure amounted to using four different separation times of 33, 66, 99, and 132 ms corresponding to images that were adjacent, every other, every third and every fourth image, respectively. Figures 5.9 through 5.16, below, demonstrate some of the differences in calculated velocity direction and magnitude that result from different separation times and filtering. As shown, the consistency of velocity vectors appears to

improve with increasing image separation time. Filtering does not appear to improve vector calculation substantially.

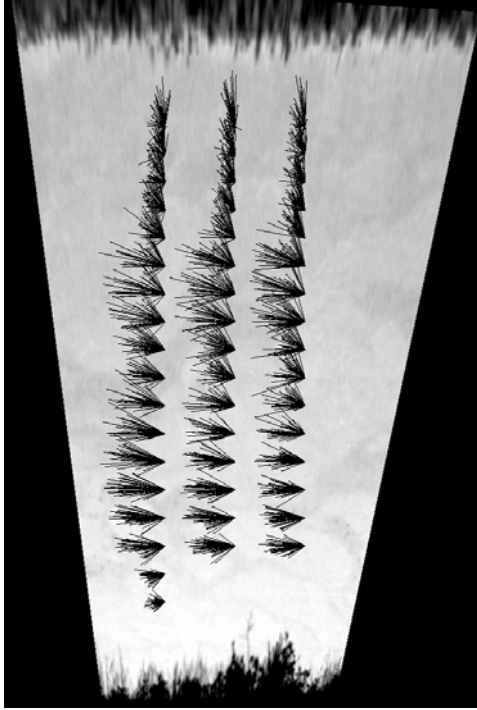


Figure 5.9 No filter, 33ms separation

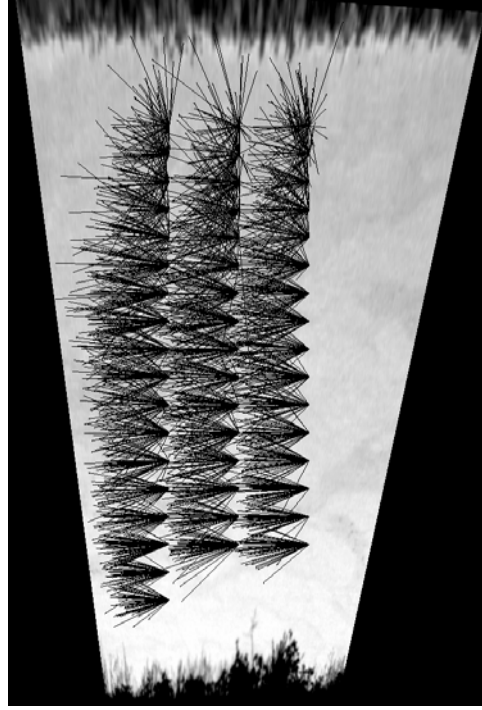


Figure 5.10 Filtered, 33ms separation

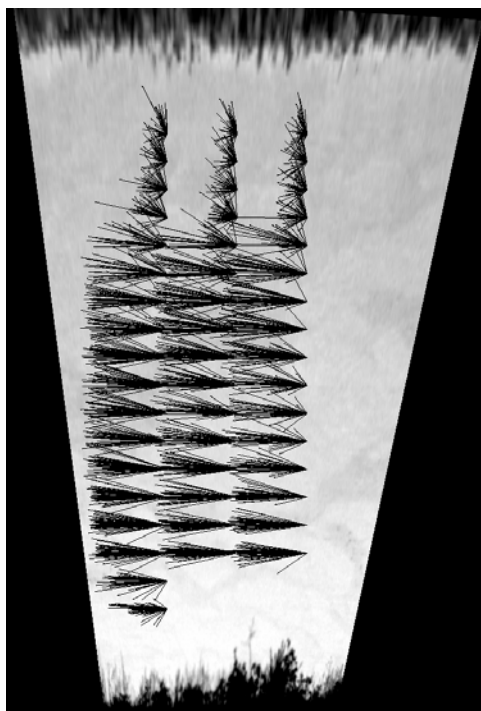


Figure 5.11 No filter, 66ms separation

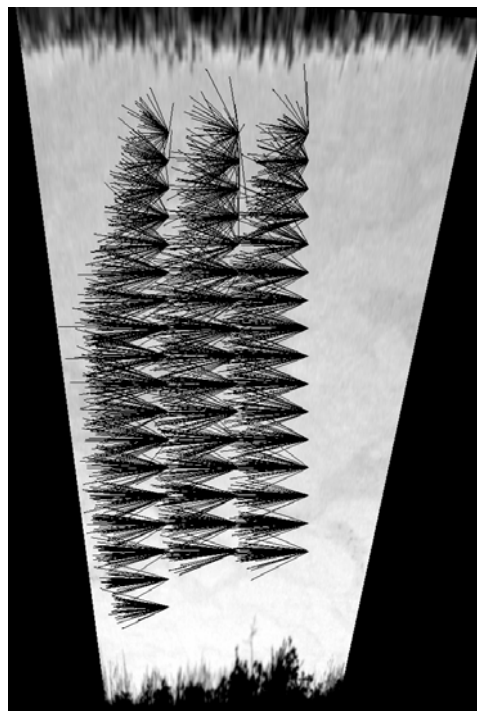


Figure 5.12 Filtered, 66ms separation

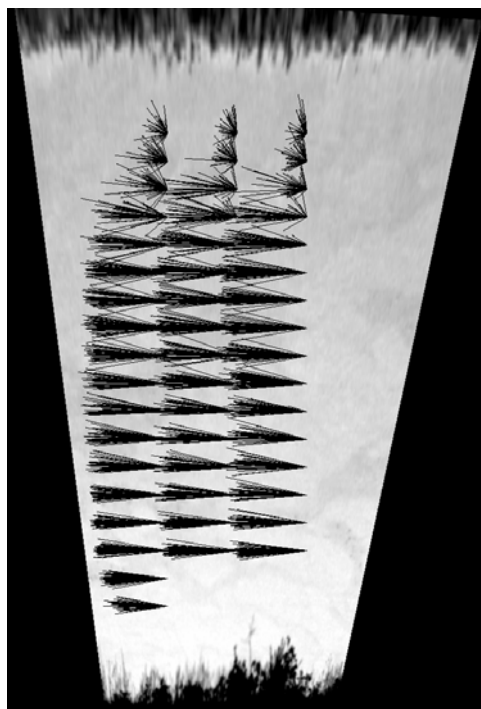


Figure 5.13 No filter, 99ms separation

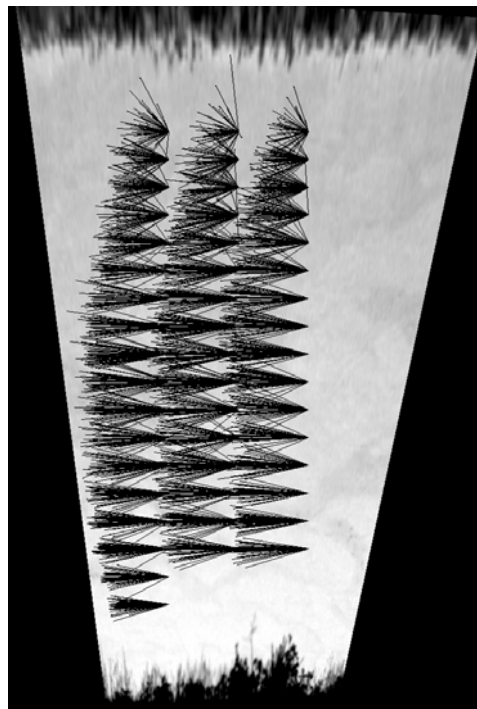


Figure 5.14 Filtered, 99ms separation

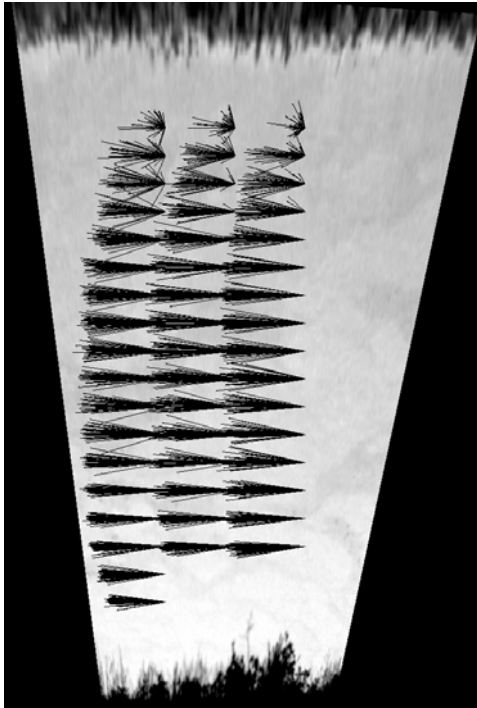


Figure 5.15 No filter, 132ms separation

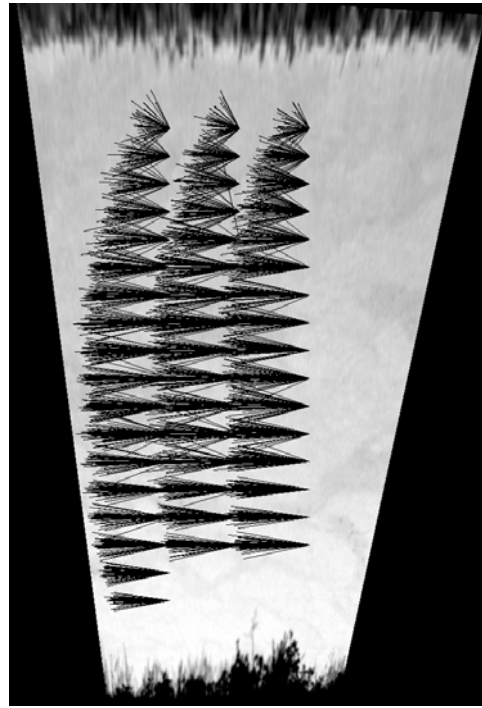


Figure 5.16 Filtered, 132ms separation

To calculate the discharge of the canal using the processed surface velocities the profile of the canal needed to be known. A profile was provided to us by the Nebraska Public Power District (NPPD). Figure 5.17 gives the profile of the canal as viewed from upstream, for reference the camera was located on the left descending bank of the canal. On the day of the tests the depth of the canal was determined to be 3.14 m (10.33 ft) and had a width of 22.58 m (74.08 ft). The discrepancy between the 24.4 m (80 ft) width measured with a measuring tape and the provided width is probably because (1) the canal geometry provided by NPPD was for a cross section located a short distance upstream where the canal was slightly more narrow, (2) because the locations of the edges of the bank were uncertain since the rip-rap that lined the banks was quite large and not uniformly placed, and (3) because of some slack in the measuring tape.

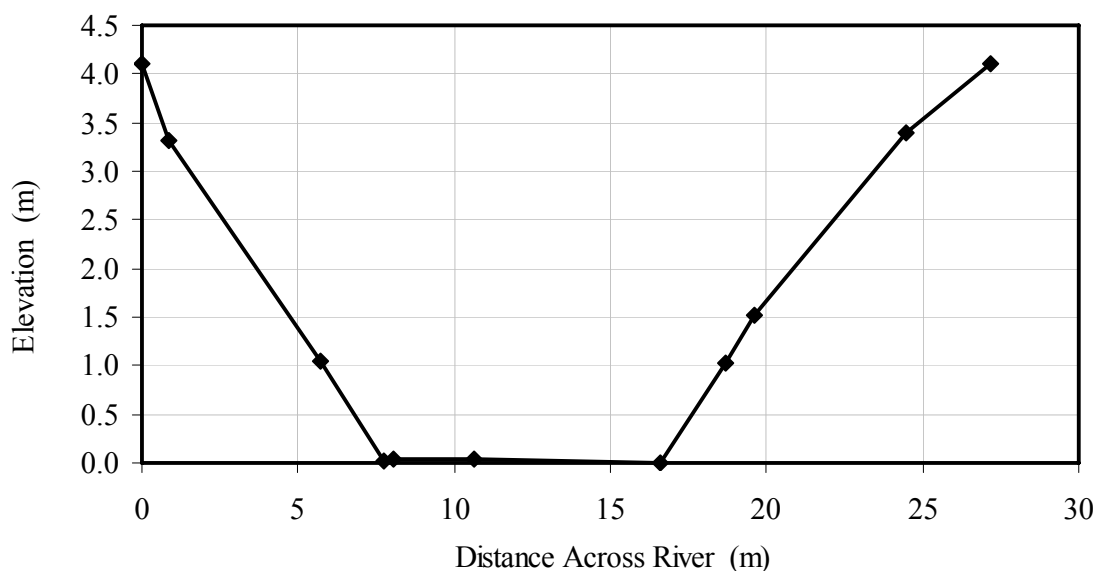


Figure 5.17 Depth profile of the NPPD power canal downstream of Sutherland Reservoir (NPPD, 2008)

Using the canal profile, the cross-sectional area under each of the surface velocity measurement points could be found. An excel spreadsheet was used to automatically find these areas in square meters. The surface velocities found by the FFCMD program in cm/s were converted to m/s. Then the product of the area under each surface velocity measurement and $7/8$ of the measured surface velocity provided the discharge of water through that area in m^3/s . The $7/8$ factor was applied because the average velocity at any position in a wide river is $7/8$ of the surface velocity at that point, according to the $1/7^{\text{th}}$ power law. Discharges were then converted to English units (ft^3/s) for comparison with NPPD's measurements. Figure 5.18 shows the differences between averaged results of 50 image pairs for each set of data. Table C.5 also gives these results. The numbers used in the legends of Figure 5.18 refer to sets of images: set numbers with an "F" suffix refer to filtered images.

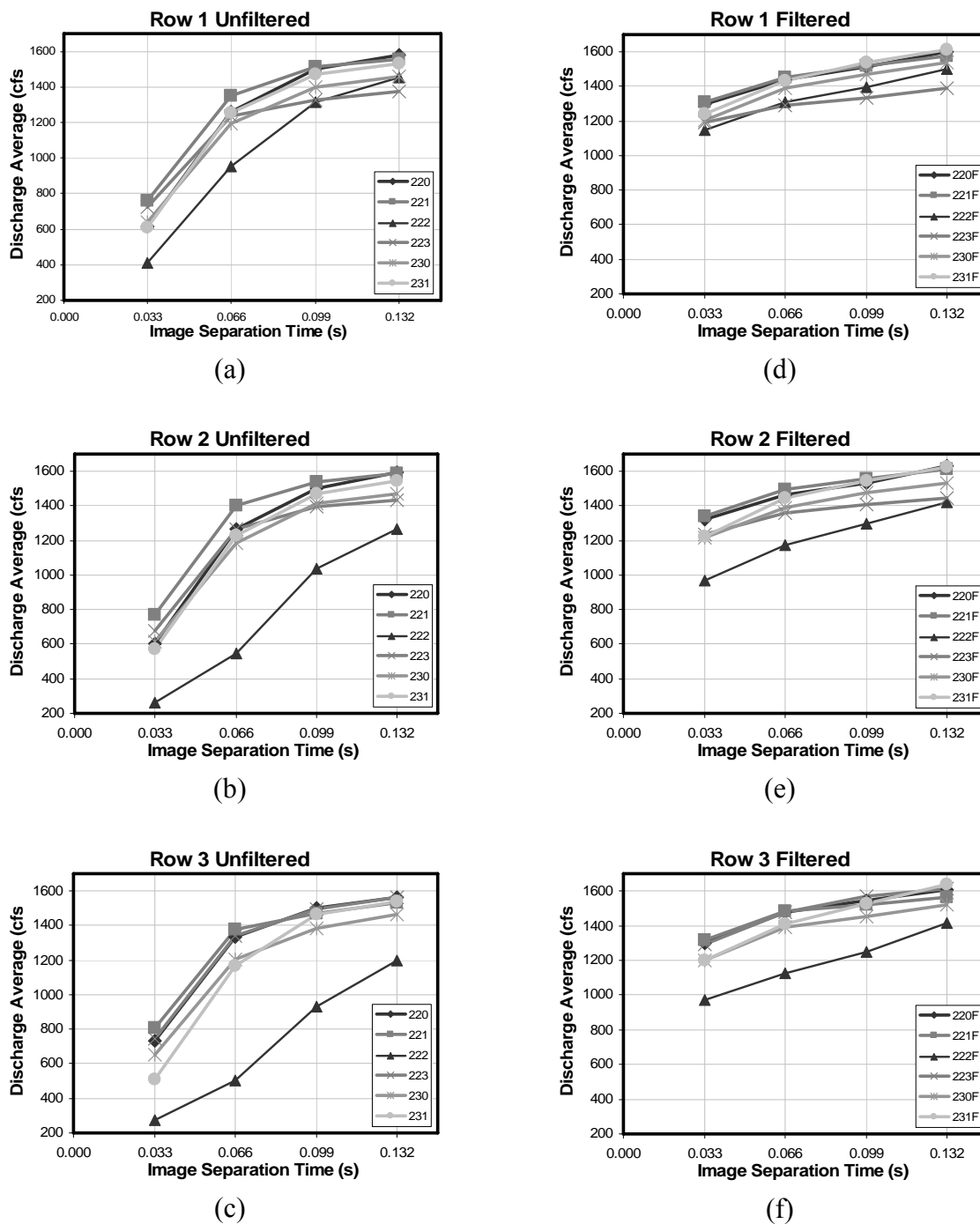


Figure 5.18 Average discharge for 50 sets of images for three transect rows. a through c show unfiltered data and d through f show filtered data.

As shown in Figures 5.15 and 5.16, velocity calculation points do not span the entire width of the canal. The reason for the space between the banks and the nearest

interrogation points is to prevent vegetation from affecting velocity measurements. If an interrogation area contains vegetation or other stationary objects, the resulting velocity calculation is usually biased to zero, especially when the stationary objects have a temperature that is significantly different than that of the water surface, causing them to have a strong influence on the MQD calculation. To account for the lack of velocity information near each edge of the canal, the velocity vectors nearest the edge were used to get an estimate of the edge discharge. Assuming that the velocity near the bank was linearly distributed from zero to the velocity at the nearest measurement location, the cross sectional area of the edge region was multiplied by half the measured velocity to get an estimate of the edge discharge. The discharge calculated for the edges of the canal accounted for less than 4% of the total flow. Thus, error in discharge estimates associated with the edges did not significantly affect total discharge calculations.

5.5 Flow Rate Comparisons, August 2008

Unfortunately on the day that most of the 2008 side view flow data were collected (8-6-08) the NPPD recording station located at the entrance to the canal was not operating. Flow data were therefore provided by the NPPD from a recording station at the downstream end of the canal, the data from the two recording stations are similar, but there is roughly an eight hour travel time for the water to travel from the canal entrance to the downstream end. Thus, the flow rate must be constant for a long period of time for flows to be considered the same at the upstream and downstream ends. The data provided by NPPD were checked and it was found that the discharge had been constant

for a long period prior to collecting the flow data. Therefore, we trusted the measured flow rates to be accurate.

Differences between the flow rate calculated using PIV and the provided flow rate can be caused by a variety of things. The uncertainty of the data provided by the NPPD was about 10%, and was also not from the nearest measuring station. Bathymetry of the bottom of the canal was not exact, though we expect that it was close. For analysis purposes all of the calculated transects across the canal were assumed to have the same bathymetry as the section located approximately 200 m upstream provided by NPPD. We have some ADCP data collected in 2009 to verify the bathymetry provided by NPPD, but the data are for a lower discharge (and thus a lower flow depth) and provides an incomplete picture of the depth profile of the channel for 2008. However, the bathymetry provided in Figure 5.17 and the ADCP bathymetry are very similar, although the sides of the canal cross section given in Figure 5.17 are somewhat steeper.

It is also possible that flow rates in the canal are not completely constant; the outlet gate of Sutherland Reservoir may allow some variation of flow. Changes in the surface elevation of the lake due to wind and waves, and unsteadiness in the conveyance structure downstream of the gate due to air entrainment does have some effect on the steadiness of the flow. We estimate that the gate setting is also accurate to about 10%.

The average of the flow rates provided by NPPD that corresponded to the time period over which the thermal imagery was gathered was 1415 cfs. Comparing the NPPD

average with the calculated discharges provides an estimate of the accuracy of the testing methods using different time separations, as shown in Table 5.1 provided below.

Table 5.1: Percentage difference of calculated flow to actual flow of 1415 cfs

Separation Time (s)	Percent difference of calculated values verse actual values	
	Unfiltered Averages	Filtered Averages
Transect 1		
0.033	-55.8	-13.0
0.066	-14.8	-2.05
0.099	0.41	3.34
0.132	5.49	8.59
Transect 2		
0.033	-58.7	-14.0
0.066	-18.8	-1.93
0.099	-1.65	3.91
0.132	4.82	9.16
Transect 3		
0.033	-56.2	-14.2
0.066	-18.4	-1.44
0.099	-2.81	4.39
0.132	4.34	10.3

The data in Table 5.1 show that the images that are 33 ms apart are not in good agreement with the averaged NPPD flow rate. This discrepancy is believed to be caused by reflections in the water biasing PIV results towards zero. Since reflections are stationary they can cause the processing routine to find the wrong MQD peak. This became a more substantial issue for data collected in 2009. Longer separation times allowed the flow to move farther between images, causing less of an influence of the zero displacement peak on the true displacement peak. Velocities could still be biased to zero, but it required much stronger reflections to do so. In general, the longer separation times produced results that were in better agreement with discharges provided by NPPD.

Another factor affecting the flow rate comparisons was the number of image pairs required to provide an accurate average discharge measurement. The analysis provided above was done using 50 pairs of images that were averaged together to get an average of the surface velocities for each run. Figure 5.19 shows that as many as 100 pairs of images are necessary before the average discharge reaches a stable value, though with 50 pairs we were always within 10% of the final value.

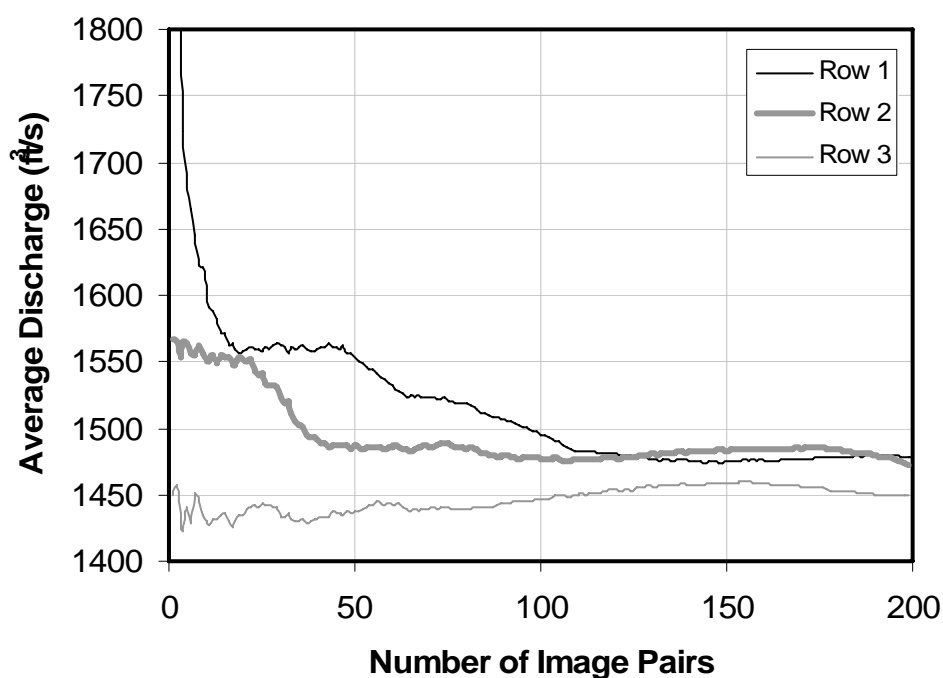


Figure 5.19 Number of image pairs required to stabilize the results for filtered image pairs in run 230.

5.6 Side View Processing Results and Comparison, July 2009

More data were collected on a second visit to the NPPD power canal on July 21 and 22, 2009. The NPPD recording station located at the entrance of the power canal was functioning on these two days at the site and was giving a discharge reading of 1160 cfs.

ADCP data gathered during the second visit gave additional information on the discharge of the canal as well as providing more information about the profile of the bottom of the canal. We did not have time to completely process the new data, so only limited amounts of data will be provided. The information collected, however, does provide some important conclusions about using thermal imagery for PIV, and provides direction for further development of the process. Thus, some of the preliminary results are presented below.

For the July 2009 side view data, a total of seven sets of test images were collected. Each set of test images was processed in the same way as the side view images collected in August of 2008, providing rectified oblique images that were both filtered and unfiltered. 50 pairs of images were compared to each other from each set of processed files for four separation times. The same four time intervals were used, separation times of 33, 66, 99, and 132 ms. Figures are provided below that when compared to Figure 5.18 help demonstrate the differences in the data collected in 2008 to 2009.

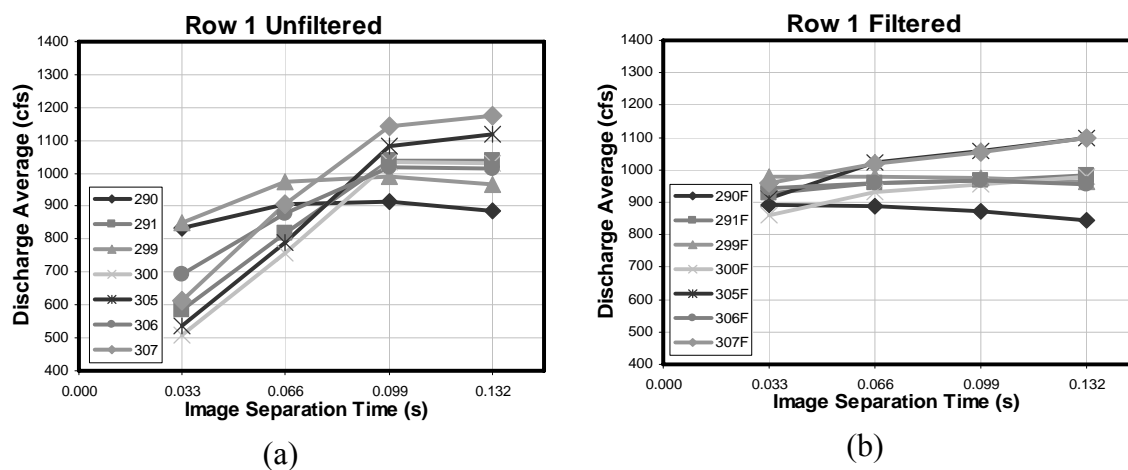


Figure 5.20 Discharge average of 50 sets of images for the first transect row.

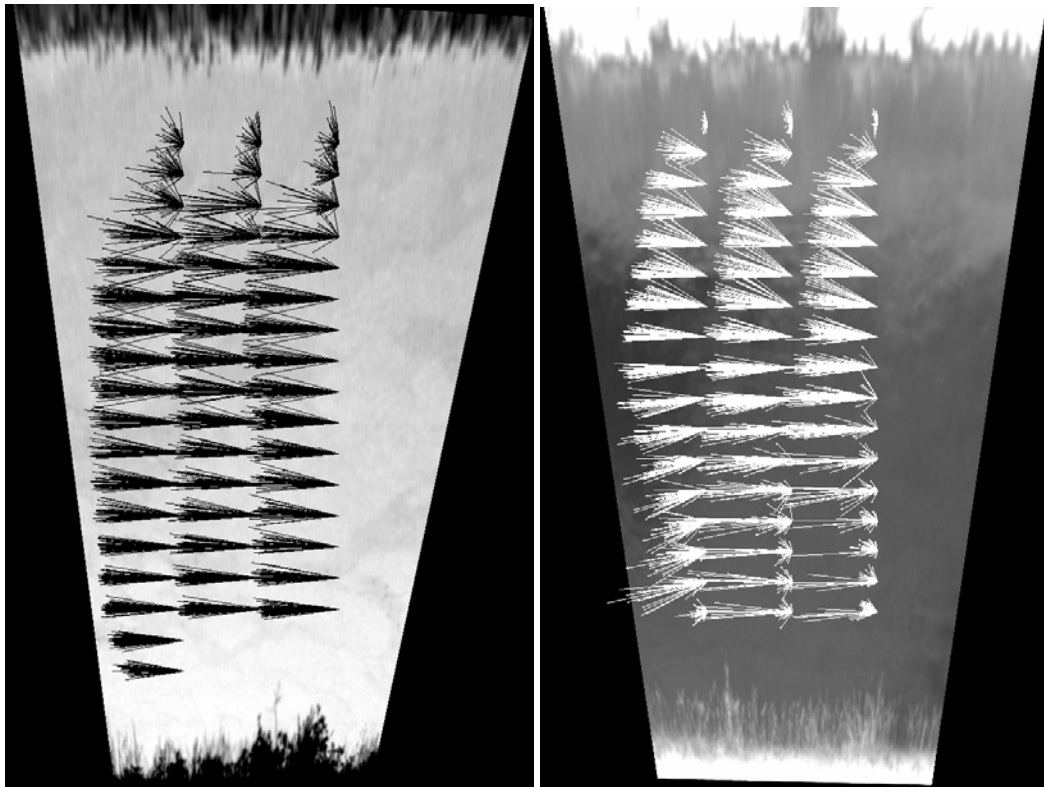
The flow measured by NPPD with a Sontek Argonaut was 1160 ft³/s, and the rated discharge of the gate was 1200 ft³/s. There is clearly much greater variability in the results than was found for the 2008 data, and all of the discharges calculated using surface velocimetry are lower than expected. Table 5.2 also provides information on the percent difference of the averaged data compared to the actual discharge of the canal of 1160 ft³/s provided by NPPD. The table reinforces the conclusion that surface velocimetry measurements were biased low. ADCP measurements at the location of the side view measurements indicated that the average discharge was 1194 ft³/s based on 12 transects, supporting NPPD's measurement.

Table 5.2: Percentage difference of calculated flow to actual flow of 1160 cfs

Separation Time (s)	Percent difference of calculated vs. actual discharge	
	Unfiltered Averages	Filtered Averages
Transect 1		
0.033	-42.5	-20.8
0.066	-26.4	-17.5
0.099	-12.7	-16.7
0.132	-13.0	-16.3

As shown in Table 5.2, the percent differences between measured discharges were not as close as the percent differences found during the tests from the previous year. The reason for the discrepancy in the percent differences from the actual discharge can be seen in the vector plots shown in Figure 5.21. Figure 5.21a shows a set of vectors determined from data collected in 2008 – a non filtered image set separated by 66 ms where the vectors are generally consistent in magnitude and have a similar direction. Figure 5.21b shows vectors from data collected in 2009 – also a non filtered set separated by 66 ms, but the vector magnitudes and directions vary significantly. Furthermore, it should be noted that

the vectors on the bottom left of the image seem to veer down. Of particular interest is the observation that some of the interrogation locations appear to have two modes, a low velocity mode and a high velocity mode.



(a) (b)
Figure 5.21 (a) Image with good vector plots with few variations in magnitude and direction. (b) Image with poor vector plots with large variation in magnitude and direction.

Since so many vectors have low magnitudes or veer in an unexpected direction it is easy to see why the average of the calculated discharges is biased low. While it is not uncommon for velocities in the flow field to vary somewhat, the near-zero velocities observed in Figure 5.21b are certainly incorrect. We suspect that the inconsistencies in the vectors are due to noise caused by infrared reflections from the water surface. These

reflections are partially visible in Figure 5.21, but are demonstrated more clearly in Figure 5.22 without the superimposed vector plots.

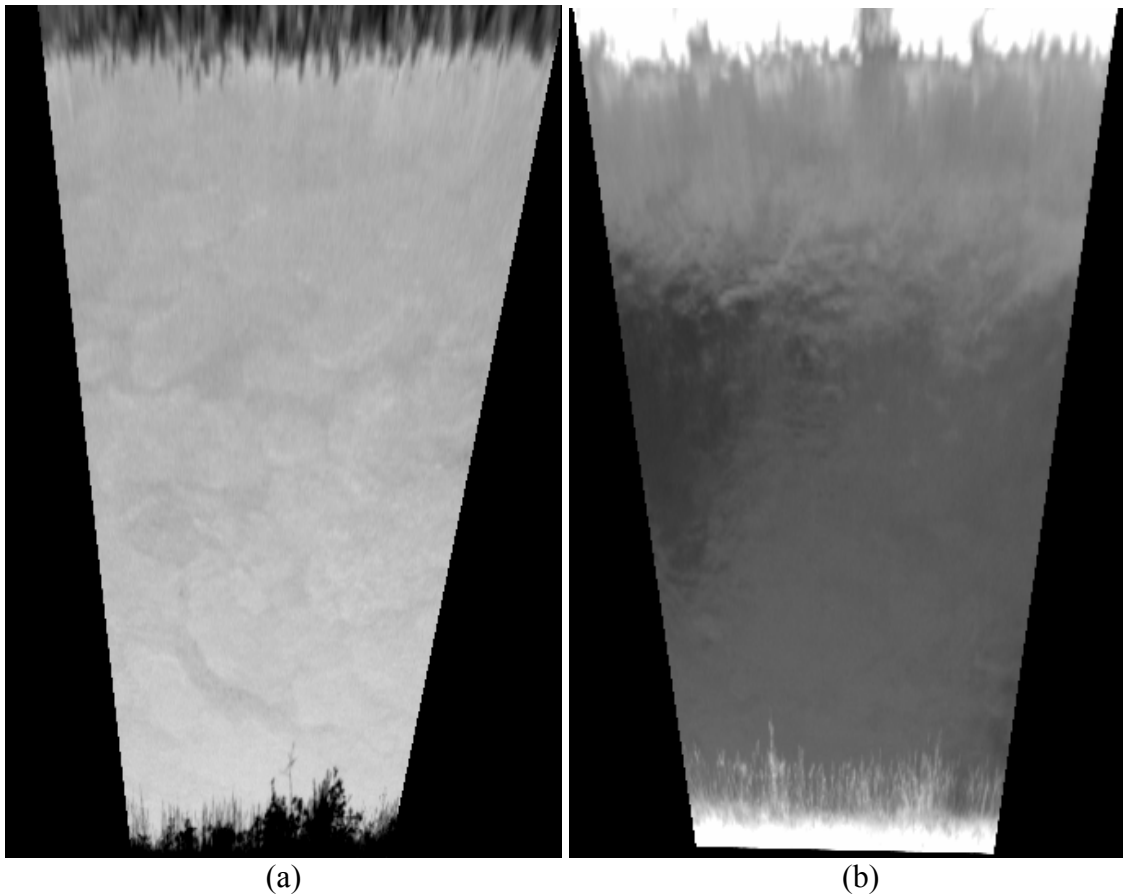


Figure 5.22 (a) Image showing few reflections with the banks cooler than the water. (b) Image showing reflections with the banks warmer than the water.

The image in Figure 5.22a shows that there were few visible reflections in the images of the August 6, 2008 data, it also shows that the banks are cooler (darker) than the canal water. The image in Figure 5.22b (July 22, 2009 data) shows many reflections on the water surface and that the banks are warmer than the water. These reflections in the water tend to bias the measurements to zero if the temperature structures on the surface of the water do not have stronger thermal radiation. It is thought that the reflections also

cause the vectors on the lower left side of the 2009 images to be incorrectly deflected toward the bank.

There is one similarity between the image comparisons of the August 6, 2008 data and the July 22, 2009 data that should be noted. The vectors in all of the image sets appear to be more inconsistent close to the upper bank of the canal in the image. This biasing is in part due to the distance of the vector calculation locations from the camera. Since interrogation locations near the upper part of the image are farther from the camera, the effective resolution of the original images is worse near the top of the image, reducing the signal to noise ratio of the MQD calculations. Bank reflections are also stronger in this part of the image. In general, it appears that vectors become less reliable at about 40 m (130 ft) from the camera for this set of data.

Chapter 6. Conclusions

6.1 Overview

The purpose of this thesis was to develop a method to measure water surface velocities using a thermal imaging camera. The work presented in this thesis focused mainly on work done at the Southerland Reservoir outlet canal, though some tests were initially done in the laboratory. The process of finding velocities and discharges from measurements with the thermal camera required aligning misaligned images, converting oblique images to images with uniform pixel sizes, testing whether or not filtering was appropriate, finding an appropriate interrogation technique, and determining the number of image pairs necessary to get a reasonable estimate of the discharge.

6.2 General conclusions

From the data presented herein there are several general conclusions that can be made. First, reflections have a great deal of influence on the velocity vectors being calculated. If the contrast of the temperature structures on the surface of the water is too low compared to reflections, the velocity calculation is biased to zero. The reflections can also cause the velocity calculations to be deflected in the wrong direction. Although we have some potential solutions to the problems the reflections create, we have not had time to test them. The first method would be to adjust the MQD code so that an image shift of zero is not possible. Essentially, the search code could check the MQD only for the region of possible velocities. The risk associated with this method is that it makes it impossible to measure very low velocities. A second option is to find a method to remove reflections from the image by removing the background image. This is not as

easy as it may sound, since removing the background image can easily introduce unwanted effects that also bias the velocities to zero. Finally, it was noted that the reflections played a much more significant role when the water was cold relative to the banks than when it was warm relative to the banks. It may be that this method must be restricted to times of the day when the water temperature is relatively warm or can only be applied at angles where reflections are minimal.

When reflections were not a problem, the average stabilizing data showed that the 50 sets of images used to calculate the average discharges can give a good approximation of the actual average discharge. The average stabilizing data also showed that the accuracy of the average discharge can be improved if 100 to 115 sets of images are averaged together.

Other factors affecting the accuracy of the results that were studied were the image separation compared to the velocity of the flow. If there was not enough movement from the first to the second image of a set the results tended to be biased to zero. The observation of translation distance compared to image separation will also have implications on the usable working distance of the IR camera from the water body being observed because as the IR camera is moved farther from a water body, the apparent velocity of the water is reduced. It was noted that near the banks, where velocities were lower, larger separation times were necessary to allow thermal structures to move far enough so that velocities were not biased to zero. This problem was amplified by the fact that the strongest reflections were generally near the banks.

6.3 Implications for future research

For this method to become more reliable certain aspects of the processing method need to be studied. Most importantly, a new process must be developed in an attempt to remove the zero bias of reflections out of the images. Reflections can not always be avoided and should be expected at almost any field site where this method can be used, though using the device at night when solar reflections are negligible may be an option. A distinct advantage of removing the zero bias of reflections, if it can be done, is that it will allow for increased sensitivity of the vector calculations, this would be especially useful for low contrast images.

The relation between the velocity of the water and image separation should be more thoroughly studied, so that the user can select an appropriate image separation time based on flow velocities and camera and site geometry. Also it would be beneficial to develop a more accurate understanding of the distance limitations of this method. Using the streamwise view images that we collected, we had hoped to do that, but unfortunately, we did not have the time necessary to complete this process. Knowing these limitations would allow this method to be appropriately applied with IR cameras of varying resolution and at a range of viewing distances and angles.

References

- Admiraal, D.M., Stansbury, J.S. and Haberman, C.J., (2004) "Case Study: Particle Velocimetry in a Model of Lake Ogallala." *Journal of Hydraulic Engineering*, **130** (7), 599-607.
- Bramson, M.A., (1968) Infrared Radiation, a Handbook for Applications, Ed. William L. Wolfe, Plenum Press, NY. 623 pp.
- Canaday Station outlet canal map, retrieved in August 2009 from website <http://maps.google.com/>
- Clark, Matt. (2009) *Physical Model of a Combined Weir, Sluice Gate, and Culvert Control Structure*, unpublished thesis (M.S.), University of Nebraska at Lincoln.
- Cowen, Edwin A. (2000) "The subtleties of making accurate measurements with PIV," paper presented at *Building Partnerships*, ASCE/EWRI Water Resources Conference, Minneapolis, Minnesota, July 30-August 2, 2000
- Ettema, R., Fujita, I., Muste, M., and Kruger, A. (1997). "Particle-Image Velocimetry for Whole-Field Measurement of Ice Velocities," *Cold Regions Science and Technology Journal*, **26(2)**, 97-112
- FLIR Systems, Inc. (2006) FLIR Systems ThermaCAM S65 HS, Technical Documentation. FLIR Systems, Wilsonville, OR
- FLIR Systems, Inc. (2008, August) FLIR ThermaCAM S65 Infrared Camera. Retrieved from FLIR Systems website: http://www.flir.com.hk/S65_print.htm

- Fujita, I., Aya, S. and Deguchi, T. (1997) "Surface velocity measurement of river flow using video images of an oblique angle," *Proceedings XXVIIIth IAHR Conference, Theme B, Vol. I*, San Francisco, CA, 227-232.
- Fujita, I., Muste, M. and Kruger, A. (1998) "Large-scale particle image velocimetry for flow analysis in hydraulic engineering applications," *Journal of Hydraulic Research*, **36(3)**, 397-414.
- Guezennec, Y. G. and Kiritsis, N. (1990) "Statistical investigation of errors in particle image velocimetry," *Experiments in Fluids*, **10**, 138-146.
- Gui, L. and Merzkirch, W. (2000) "A comparative study of the MQD method and several correlation-based PIV evaluation algorithms," *Experiments in Fluids*, **28**, 36-44.
- Hetsroni G., Kowalewski T. A., Hu B. and Mosyak A. (2001) "Tracking of coherent thermal structures on a heated wall by means of infrared thermography," *Experiments in Fluids*, **30**, 286-294.
- Jähne, B. and Haußecker, H. (1998) "Air-water gas exchange," *Annual Review of Fluid Mechanics*, **30**, 443-468.
- Jessup A.T. and Phadnis, K R (2005) "Measurement of the geometric and kinematic properties of microscale breaking waves from infrared imagery using a PIV algorithm," *Measurement Science and Technology*, **16**, 1961-1969.
- Lake Ogallala inlet map, retrieved in August 2009 from website <http://maps.google.com/>
- Linder, David. Personal communication of NPPD depth profile information, August 2008
- Meadows, G., Lyzenga, D., Beck, R., and Lyden, J. (1991) "Nonintrusive, multi-point measurements of water surface slope, elevation and velocity," Eighteenth Symposium

- on Naval Hydrodynamics, Commission on Physical Sciences, Mathematics, and Applications (CPSMA), National Academy Press, Washington, D.C. 852 pp.
- McAlister, E.D. (1964) "Infrared-Optical Techniques Applied to Oceanography 1. Measurement of Total Heat Flow from the Sea Surface," *Applied Optics*, **3(5)**, 609-612.
- Schemper, Tyler J. (2007) *A Field Study and Analysis of Velocity Fields and Turbulence Parameters on Meandering Rivers in Nebraska*, unpublished thesis (M.S.), University of Nebraska at Lincoln.
- Sokkisha Co., LTD. (2005) Sokkia Set5/Set5S Electronic Total Station, Operator's Manual. Sokkisha Co., LTD., Tokyo, Japan
- SonTek (1997) SonTek ADV Field Acoustic Doppler Velocimeter, Technical Documentation. SonTek, San Diego, CA.
- Sutherland Reservoir map, retrieved in August 2009 from website <http://maps.google.com/>
- Sutherland Reservoir outlet map, retrieved in August 2008 from website <http://maps.google.com/>
- Willert, C. E. and Gharib, M. (1991) "Digital particle image velocimetry," *Experiments in Fluids*, **10**, 181-193.
- Zhang, X. and Harrison, S. (2004) "A laboratory observation of the surface temperature and velocity distributions on a wavy and windy air-water interface," *Physics of Fluids*, **16(1)**, L5-L8.

Appendix A

Small Flume Flow Rate Data

Table A.1: Flow rate average of the runs, measured using the V-notch Weir.

Test	Weir Height	Flow Rate	Upstream Depth	Downstream Depth	Seed Pulse Cycle/Width	Bulk Water Temp.
	(inches)	(cfs)	(cm)	(cm)	(s)/(s)	(°C)
A.1.1	2	0.4337	7.28	8.02	30/5	20.8
A.1.2	2	0.4311	7.29	8.48	20/5	20.8
A.1.3	2	0.4328	7.29	8.53	10/5	20.8
A.1.4	2	0.4303	7.21	8.54	NA	20.9
A.2.1	3.5	0.4515	10.36	11.72	30/5	20.6
A.2.2	3.5	0.4367	10.35	11.72	20/5	20.6
A.2.3	3.5	0.4476	10.32	11.74	10/5	20.7
A.2.4	3.5	0.4393	10.32	11.69	NA	20.7
A.3.1	6.5	0.4167	18.81	20.16	30/5	20.7
A.3.2	6.5	0.4218	18.83	20.18	20/5	20.8
A.3.3	6.5	0.4171	18.81	20.16	10/5	20.9
A.3.4	6.5	0.4188	18.91	20.19	NA	20.8
A.4.1	9.25	0.4251	26.00	27.25	30/5	19.8
A.4.2	9.25	0.4260	25.87	27.15	20/5	20.1
A.4.3	9.25	0.4256	25.88	27.27	10/5	20.3
A.4.4	9.25	0.4226	25.87	27.26	NA	20.4
A.5.1	11.5	0.4154	30.92	32.19	30/5	20.5
A.5.2	11.5	0.4192	30.93	32.27	20/5	20.5
A.5.3	11.5	0.4201	30.90	32.24	10/5	20.6
A.5.4	11.5	0.4150	30.92	32.17	NA	20.7
B.1.1	2	0.1011	4.41	5.77	30/5	21.2
B.1.2	2	0.1014	4.40	5.78	20/5	21.3
B.1.3	2	0.1016	4.41	5.76	10/5	21.3
B.1.4	2	0.1005	4.37	5.68	NA	21.4
B.2.1	3.5	0.0989	7.51	8.91	30/5	21.5
B.2.2	3.5	0.0978	7.53	8.86	20/5	21.5
B.2.3	3.5	0.0995	7.53	8.88	10/5	21.5
B.2.4	3.5	0.1180	7.49	8.80	NA	21.6

Table A.1: (Continued)

Test Group	Weir Height	Flow Rate	Upstream Depth	Downstream Depth	Seed Pulse Cycle/Width	Bulk Water Temp.
	(inches)	(cfs)	(cm)	(cm)	(s)/(s)	(°C)
B.3.1	6.5	0.0996	15.67	17.04	10/5	21.7
B.3.2	6.5	0.1005	15.66	17.01	30/5	21.7
B.3.3	6.5	0.0991	15.64	17.01	60/5	21.7
B.3.4	6.5	0.0998	15.62	16.98	NA	21.8
B.4.1	9.25	0.0947	23.24	24.55	60/5	21.9
B.4.2	9.25	0.0964	23.27	24.60	30/5	21.9
B.4.3	9.25	0.0979	23.25	24.60	105	21.9
B.4.4	9.25	0.0960	23.21	24.57	NA	22.0
B.5.1	11.5	0.0968	28.03	29.37	60/5	22.1
B.5.2	11.5	0.0965	28.06	29.38	30/5	22.1
B.5.3	11.5	0.0975	28.05	29.43	105	22.1
B.5.4	11.5	0.0932	28.09	29.36	NA	22.1
C.1.1	2	0.9892	10.57	11.69	30/5	21.7
C.1.2	2	0.9760	10.56	11.67	20/5	21.7
C.1.3	2	0.9746	10.52	11.62	10/5	21.7
C.1.4	2	0.9830	10.51	11.64	NA	21.7
C.2.1	3.5	0.9788	14.10	15.39	30/5	21.6
C.2.2	3.5	0.9746	14.20	15.42	20/5	21.7
C.2.3	3.5	0.9837	14.16	15.39	10/5	21.7
C.2.4	3.5	0.9830	14.09	15.39	NA	21.7
C.3.1	6.5	0.9936	22.61	23.87	30/5	21.6
C.3.2	6.5	0.9872	22.58	23.88	20/5	21.6
C.3.3	6.5	0.9894	22.59	23.83	10/5	21.6
C.3.4	6.5	0.9901	22.62	23.82	NA	21.6
C.4.1	9.25	0.9929	29.48	30.78	30/5	21.5
C.4.2	9.25	0.9901	29.50	30.75	20/5	21.5
C.4.3	9.25	0.9872	29.56	30.83	10/5	21.5
C.4.4	9.25	0.9936	29.52	30.77	NA	21.6

Table A.1: (Continued)

Test Group	Weir Height	Flow Rate	Upstream Depth	Downstream Depth	Seed Pulse Cycle/Width	Bulk Water Temp.
	(inches)	(cfs)	(cm)	(cm)	(s)/(s)	(°C)
C.5.1	11.5	0.9893	35.42	36.61	30/5	21.5
C.5.2	11.5	0.9887	35.39	36.61	20/5	21.5
C.5.3	11.5	0.9922	35.33	36.58	10/5	21.5
C.5.4	11.5	0.9858	35.34	36.58	NA	21.5
D.1.1	2	1.5387	13.09	14.06	30/5	21.2
D.1.2	2	1.5323	13.08	14.07	20/5	21.2
D.1.3	2	1.5544	13.05	14.25	10/5	21.2
D.1.4	2	1.5405	12.99	14.19	NA	21.2
D.2.1	3.5	1.5405	16.73	18.02	30/5	21.2
D.2.2	3.5	1.5516	16.67	18.13	20/5	21.2
D.2.3	3.5	1.5461	16.78	18.00	10/5	21.2
D.2.4	3.5	1.5470	16.69	18.02	NA	21.3
D.3.1	6.5	1.5378	25.41	26.62	30/5	21.3
D.3.2	6.5	1.5341	25.24	26.56	10/5	21.3
D.3.3	6.5	1.5304	25.17	26.66	5/5	21.4
D.3.4	6.5	1.5277	25.18	26.58	NA	21.4
D.4.1	9.25	1.7153	32.53	33.91	20/10	21.4
D.4.2	9.25	1.5222	32.51	33.75	10/10	21.4
D.4.3	9.25	1.5268	32.54	33.74	5/5	21.4
D.4.4	9.25	1.5240	32.60	33.84	NA	21.4
D.5.1	11.5	1.5222	38.22	NA	20/10	21.4
D.5.2	11.5	1.5195	38.19	NA	10/10	21.4
D.5.3	11.5	1.5304	38.18	NA	5/5	21.4
D.5.4	11.5	1.5222	38.26	NA	NA	21.4
E.1.1	2	2.2157	15.74	17.05	20/10	21.4
E.1.2	2	2.2220	15.88	17.18	10/10	21.4
E.1.3	2	2.2163	15.85	17.01	5/5	21.4
E.1.4	2	2.1935	15.75	16.96	NA	21.4

Table A.1: (Continued)

Test Group	Weir Height	Flow Rate	Upstream Depth	Downstream Depth	Seed Pulse Cycle/Width	Bulk Water Temp.
	(inches)	(cfs)	(cm)	(cm)	(s)/(s)	(°C)
E.2.1	3.5	2.1890	19.49	21.06	20/10	21.4
E.2.2	3.5	2.1844	19.41	21.07	10/10	21.5
E.2.3	3.5	2.1461	19.27	20.69	5/5	21.5
E.2.4	3.5	2.1517	19.33	20.77	NA	21.5
E.3.1	6.5	2.1193	28.08	29.44	20/10	21.5
E.3.2	6.5	2.1137	28.17	29.79	10/10	21.5
E.3.3	6.5	2.1237	28.24	29.69	5/5	21.6
E.3.4	6.5	2.1528	28.21	29.91	NA	21.6
E.4.1	9.25	2.1137	35.16	36.83	20/10	21.6
E.4.2	9.25	2.0926	35.12	36.76	10/10	21.6
E.4.3	9.25	2.0761	35.19	36.88	5/5	21.6
E.4.4	9.25	2.0838	35.13	36.81	NA	21.6
E.5.1	11.5	2.0695	40.94	42.90	20/10	21.7
E.5.2	11.5	2.0761	40.85	42.50	10/10	21.7
E.5.3	11.5	2.0706	40.87	42.54	5/5	21.7
E.5.4	11.5	2.0651	40.95	42.51	NA	21.7

Appendix B

Large Flume Flow Rate Data

Table B.1: IR Camera Recording Data

Test Run	Laser Sweep Frequency	Laser Mode / Power	Data File Name	Water Temperature
	(Hz)	Mode / (W)		°C
1	NA	NA	Run 1.SEQ	20
2	0	00 / 4	Run 2.SEQ	20
3	½	00 / 4	Run 3.SEQ	20
4	1	00 / 4	Run 4.SEQ	20
5	1	00 / 4	Run 5.SEQ	20
6	1	00 / 4	Run 6.SEQ	20
7	½	00 / 4	Run 7.SEQ	20
8	½	00 / 4	Run 8.SEQ	20
9	0	00 / 4	Run 9.SEQ	20
10	0	00 / 4	Run 10.SEQ	20
11	NA	NA	Run 11.SEQ	20
12	NA	NA	Run 12.SEQ	20
Grid at \approx water surface height, 17 cm			Grid 1.SEQ	NA
Augmented grid			Grid 2.SEQ	NA

Table B.2: ADV Data

ADV Run	Point Gauge Reading	ADV Center Depth	Data File Name	Water Temperature
	(cm)	(cm)		°C
1	35.07	3.34	Run 1.adv	20
2	36.10	4.37	Run 2.adv	20
3	37.10	5.37	Run 3.adv	20
4	38.10	6.37	Run 4.adv	20
5	39.10	7.37	Run 5.adv	20
6	40.10	8.37	Run 6.adv	20
7	41.10	9.37	Run 7.adv	20
8	42.10	10.37	Run 8.adv	20
9	43.10	11.37	Run 9.adv	20
10	44.10	12.37	Run 10.adv	20

Table B.3: Large flume flow and depth data

Recording time	Flow Rate	First Point Gauge Depth	Second Point Gauge Depth	Third Point Gauge Depth	Water Temperature
	(cfs)	(cm)	(cm)	(cm)	(°C)
Before IR Data	.7790	16.70	16.75	16.86	20.0
Between IR and ADV Data	.7814	16.74	16.78	16.93	20.0
After ADV Data	.7845	16.75	16.80	16.92	20.0

Appendix C

Position reference point Data For Field Experiments

Table C.1: Ogallala Inlet Total Station Calibration Measurements August 2008

Calibration Point	Vertical Angle	Horizontal Angle	Horizontal Distance	Vertical Distance	Hypotenuse
1	96° 46' 50"	60° 46' 30"	1450.9	-172.5	1461.1
2	96° 14' 30"	64° 33' 40"	1190.4	-172.4	1202.9
3	98° 53' 20"	62° 16' 30"	1102.3	-172.4	1115.7
4	98° 46' 00"	87° 15' 30"	1117.8	-172.4	1131.0
5	96° 37' 50"	84° 58' 50"	1482.8	-172.4	1492.8
6	97° 35' 00"	85° 52' 20"	1294.6	-172.4	1306.1
7	95° 31' 00"	77° 36' 40"	1752.5	-172.4	1760.9

Table C.2: Ogallala Inlet GPS Coordinates August 2008

Calibration Point	Corresponding GPS Coordinates	
	N	W
1	41° 12.787'	101° 39.950'
2	41° 12.753'	101° 39.989'
3	41° 12.753'	101° 40.012'
4	41° 12.680'	101° 39.977'
5	41° 12.694'	101° 39.899'
6	41° 12.687'	101° 39.941'
7	41° 12.736'	101° 39.852'

Table C.3: Sutherland Reservoir Outlet Total Station Points for Upstream Images August 2008

Calibration Point	Vertical Angle	Horizontal Angle	Horizontal Distance	Vertical Distance	Hypotenuse
1	95° 33' 10"	293° 11' 20"	355.3	-34.5	356.9
2	93° 46' 40"	291° 02' 00"	521.8	-34.5	522.9
3	92° 32' 30"	289° 56' 20"	774.1	-34.4	774.9

Table C.4: Sutherland Reservoir Outlet Total Station Points for Side Images August 2008

Calibration Point	Vertical Angle	Horizontal Angle	Horizontal Distance	Vertical Distance	Hypotenuse
1	102° 38' 50"	280° 51' 20"	156.5	-35.1	160.4
2	102° 42' 10"	277° 57' 50"	155.7	-35.1	159.7
3	102° 55' 30"	272° 13' 20"	153.2	-35.2	157.2
4	102° 52' 50"	269° 11' 20"	153.8	-35.2	157.8
5	102° 48' 30"	266° 16' 20"	154.3	-35.1	158.2
6	102° 41' 00"	263° 32' 40"	155.9	-35.1	159.8
7	113° 58' 00"	88° 44' 30"	79.1	-35.2	86.6
8	114° 07' 40"	263° 12' 20"	79.1	-35.2	86.6
9	113° 34' 30"	281° 26' 10"	81.2	-35.2	88.5

Table C.5: Average discharge of 50 sets for every test run August 2008

Separation Time (s)	Averaged Discharges (cfs)					
	220	220F	221	221F	222	222F
Row 1						
0.033	617.2439	1297.052	757.7528	1308.562	408.209	1148.513
0.066	1259.908	1439.5	1350.764	1450.378	955.8047	1311.297
0.099	1500.473	1513.016	1510.3	1517.863	1315.563	1399.187
0.132	1580.506	1603.734	1557.103	1577.917	1450.677	1499.489
Row 2						
0.033	605.1202	1319.416	773.0373	1342.634	262.2665	967.5564
0.066	1264.537	1462.615	1399.766	1497.995	549.3213	1171.837
0.099	1502.361	1533.424	1536.536	1558.297	1034.258	1299.008
0.132	1595.678	1631.628	1588.116	1611.646	1264.797	1420.384
Row 3						
0.033	730.2141	1300.889	809.6807	1315.146	273.9547	973.6328
0.066	1334.647	1475.761	1377.118	1481.372	506.0914	1126.864
0.099	1503.33	1543.149	1473.604	1521.046	931.8964	1247.618
0.132	1563.716	1609.016	1535.351	1564.761	1196.529	1417.03

Table C.5: (Continued)

Separation Time (s)	Averaged Discharges (cfs)					
	223	223F	230	230F	231	231F
Row 1						
0.033	724.5849	1190.411	638.7971	1206.524	609.5098	1238.64
0.066	1236.627	1289.829	1193.634	1388.859	1256.124	1436.018
0.099	1326.21	1337.352	1399.768	1469.632	1472.244	1536.617
0.132	1376.012	1388.385	1458.48	1536.65	1533.139	1613.489
Row 2						
0.033	679.7766	1235.927	617.1364	1213.607	569.7425	1225.248
0.066	1266.246	1356.532	1183.768	1392.241	1229.088	1445.007
0.099	1393.932	1405.658	1414.735	1479.059	1467.771	1546.687
0.132	1434.26	1445.003	1469.277	1532.552	1547.09	1626.402
Row 3						
0.033	746.527	1295.354	649.8065	1198.332	510.3171	1198.874
0.066	1342.319	1480.084	1204.68	1393.583	1165.951	1410.087
0.099	1492.783	1570.74	1384.048	1450.688	1465.603	1529.308
0.132	1563.245	1613.188	1461.57	1522.168	1538.444	1635.522

Table C.6: Sutherland Reservoir Outlet Total Station Points for Side Images July 2009

North Side of Canal										
Pt.	Location	Vert. Dist.	Horz. Dist.	Hypotenuse	Vertical Angle			Horiz. Angle		
		(ft)	(ft)		Deg	Min	Sec	Deg	Min	Sec
9N	North West	-31.8	73.5	80.1	113	23	30	197	41	30
8N	North Middle	-31.9	72.2	78.9	113	49	40	188	40	10
7N	North East	-31.8	74.4	80.9	113	10	10	179	27	10

South Side of Canal										
Pt.	Location	Vert. Dist.	Horz. Dist.	Hypotenuse	Vertical Angle			Horiz. Angle		
		(ft)	(ft)		Deg	Min	Sec	Deg	Min	Sec
10S	South West	-31.8	155.1	158.3	101	35	40	197	43	50
9S	South 4 th Pt.	-31.7	152.5	155.8	101	45	20	193	27	50
8S	South Middle	-31.8	152.3	155.5	101	46	40	189	17	20
7S	South 2 nd Pt.	-31.8	151.9	155.2	101	48	20	185	40	20
6S	South East	-31.8	151.9	155.2	101	49	20	181	04	20

Table C.7: Sutherland Reservoir Outlet GPS Coordinates July 2009

North Side of Canal						
Pt.	Location	SEQ File	GPS Pts	GPS Location		Time
				North	West	
9N	North West	287	322, 323, 324	N 41° 6.213'	W 101° 6.018'	
8N	North Middle	288	325, 326, 327	N 41° 6.212'	W 101° 6.016'	
7N	North East	289	328, 329, 340	N 41° 6.212'	W 101° 6.014'	

South Side of Canal						
10S	South West	292 ¹ 298 ²	331, 332, 333	N 41° 6.200'	W 101° 6.026'	2:19
9S	South 4 th Pt.	293	334, 335, 336	N 41° 6.200'	W 101° 6.024'	
8S	South Middle	294	337, 338, 339	N 41° 6.201'	W 101° 6.023'	
7S	South 2 nd Pt.	295	340, 341, 342	N 41° 6.199'	W 101° 6.021'	
6S	South East	296 ³ 297	343, 344, 345	N 41° 6.199'	W 101° 6.018'	2:16

Note that north side positions are positions of bank edge, but that the water surface cannot be seen at this location. Thus, we needed to do three additional points with the prism held out into the flow.

¹SEQ 292, flag was reversed

²SEQ 298, the flag was wetted to make it cold so that it would stand out.

³SEQ 296, not in proper position

Table C.8: Average discharge of 50 sets for every test run July 2009

Separation Time (s)	Averaged Discharges (cfs)					
Row 1	290	290F	291	291F	299	299F
0.033	835.1374	892.7696	584.3065	926.1629	850.7948	978.168
0.066	904.503	889.3295	818.1876	959.4113	974.374	977.6085
0.099	913.5281	872.72	1039.632	968.9622	992.0625	974.6333
0.132	887.6904	844.7426	1038.421	981.4673	965.947	962.1525
Row 2						
0.033	732.7123	1019.619	790.0336	857.7411	886.4907	981.2305
0.066	932.0756	1107.817	839.1185	775.5397	978.3845	972.8474
0.099	1119.812	1146.371	790.107	710.3415	988.5337	962.9976
0.132	1170.601	1213.17	685.0686	634.0783	946.7548	944.4788
Row 3						
0.033	577.8877	966.8447	843.2588	948.3096	773.6037	937.4968
0.066	791.3501	1039.858	913.868	890.5953	944.2649	959.8508
0.099	1074.93	1077.424	904.2588	842.1299	982.3413	954.7385
0.132	1111.625	1118.225	823.7331	787.6478	949.7883	937.1404

Table C.8: (Continued)

Separation Time (s)	Averaged Discharges (cfs)					
Row 1	300	300F	305	305F	306	306F
0.033	507.0416	858.3729	534.5417	912.0997	691.7725	944.7419
0.066	758.2939	931.9463	788.1395	1021.947	879.4117	959.6862
0.099	1032.704	954.4913	1081.665	1059.076	1018.333	967.4821
0.132	1032.301	981.1707	1118.834	1097.122	1015.099	955.7209
Row 2						
0.033	519.1127	968.9743	665.6369	951.9735	691.9893	1048.567
0.066	956.1568	1088.049	891.8282	1012.443	1014.737	1125.728
0.099	1187.94	1143.548	1088.372	1036.112	1255.003	1169.281
0.132	1171.256	1184.798	1072.75	1025.713	1258.272	1185.695
Row 3						
0.033	615.8525	928.4763	556.6278	888.7534	590.7963	1092.433
0.066	902.1983	973.5716	746.6998	953.622	1086.556	1230.313
0.099	1051.119	994.9431	969.1937	968.2754	1345.669	1298.761
0.132	1015.821	1000.016	972.7279	964.1768	1373.757	1344.678

Table C.8: (Continued)

Separation Time (s)	Averaged Discharges (cfs)					
	307	307F				
Row 1						
0.033	613.1666	960.7492				
0.066	904.3441	1020.624				
0.099	1141.173	1056.713				
0.132	1176.356	1097.369				
Row 2						
0.033	617.6081	905.4857				
0.066	786.8695	938.0205				
0.099	956.5433	937.0329				
0.132	967.0676	933.5983				
Row 3						
0.033	445.0336	884.3585				
0.066	586.2063	928.1963				
0.099	877.4894	963.0582				
0.132	946.6579	993.1383				

Table C.9: Three supplemental position reference points with prism held over the water in view of the infrared camera July 2009

North Side of Canal										
Pt.	Location	Vert. Dist.	Horz. Dist.	Hypotenuse	Vertical Angle			Horiz. Angle		
		(ft)	(ft)		Deg	Min	Sec	Deg	Min	Sec
9Ns	North West	-36.2	78.1	86.1	114	52	50	197	37	20
9Ns	North West				114	46	20	197	55	20
8Ns	North Middle	-36.3	77.0	85.1	115	13	20	189	24	20
7Ns	North East	-36.3	79.3	87.2	114	36	30	179	40	00

These points were gathered by holding the prism over the water out into the stream so that the prism could be seen by the camera. The prism is approximately 2 inches above the water surface. Note that one point (SEQ 301) was gathered prior to deciding that it was important to measure distance. This point gives angular location of the prism, but not the actual distance to the prism. If it was important to use this point, it should be noted that the prism is located the length of the prism pole away from point 9N over the flow.